

# Study of MFI Zeolite Membranes for CO<sub>2</sub> Separation

Shahpar Fouladvand

Chemical Technology



# Study of MFI Zeolite Membranes for CO<sub>2</sub> Separation

Shahpar Fouladvand

November 2016



Luleå University of Technology

Department of Civil, Environmental and Natural Resources Engineering

Division of Chemical Engineering

Printed by Luleå University of Technology, Graphic Production 2016

ISSN 1402-1757

ISBN 978-91-7583-703-1 (print)

ISBN 978-91-7583-704-8 (pdf)

Luleå 2016

[www.ltu.se](http://www.ltu.se)





## Abstract

Nowadays, the need and interest for renewable sources of energy has increased. Biogas is a renewable source of energy that can be considered as a sustainable substitute for natural gas. Biogas is mainly composed of CH<sub>4</sub> and CO<sub>2</sub>, and normally the CO<sub>2</sub> content of the gas has to be reduced as it decreases the calorific value of the gas and it may also cause corrosion in pipes and other equipment. Most today's technologies used for upgrading biogas have been adapted from upgrading of natural gas. However, these technologies are best suited for large scale operation; whereas, production of biogas is typically several orders of magnitude smaller. This leads to high costs for removal of CO<sub>2</sub> from biogas and consequently, new efficient technologies for upgrading biogas should be developed. Membrane-based separations are generally considered as energy efficient and are suitable for a wide range in scale of production due to their modular design. Zeolite membranes have been singled out as especially attractive membranes for gas separations. In this work, we therefore study separation of CO<sub>2</sub> from CH<sub>4</sub> and H<sub>2</sub> using zeolite MFI membranes.

The performance of a high-silica (Si/Al *ca.* 139) MFI membrane for CO<sub>2</sub>/CH<sub>4</sub> separation was investigated in a wide temperature range *i.e.* 245 K to 300 K. The separation factor increased with decreasing temperatures as is typically the case for adsorption governed separations. The highest separation factor observed was about 10 at 245 K. The CO<sub>2</sub> permeance was very high in the whole temperature studied, varying from *ca.*  $60 \times 10^{-7} \text{ mol s}^{-1} \text{ m}^{-2} \text{ Pa}^{-1}$  at the lowest temperature to about  $90 \times 10^{-7} \text{ mol s}^{-1} \text{ m}^{-2} \text{ Pa}^{-1}$  at the highest temperature studied. The CO<sub>2</sub> permeance was higher than that reported previously in the open literature for this separation. Modeling of the experimental data revealed that the membrane performance was adversely affected by pressure drop over the support, whereas the effect of concentration polarization was small. Removing the former effect would improve both the permeance and selectivity of the membrane.

In order to investigate the impact of the aluminum content on the performance of MFI membranes for the CO<sub>2</sub>/CH<sub>4</sub> separation, MFI membranes with different Si/Al ratios were prepared. Increasing the aluminum content makes the zeolite

more polar which should increase the CO<sub>2</sub>/CH<sub>4</sub> adsorption selectivity. Again the effect of temperature on the performance was investigated by varying the temperature in a range almost similar as above. Altering the Si/Al ratio in MFI zeolite membranes indeed changed the separation performances. At the lower temperatures the separation performance increased with increasing aluminum content in the zeolite as a result of larger adsorption selectivity. However, as the temperature was decreased, the selectivity of the membrane with the highest aluminum content went through a maximum, whereas for the other membranes the selectivity continued to increase with decreasing temperature under the conditions studied. At the same time, the CO<sub>2</sub> permeances were high for all membranes studied and for the membrane with the highest selectivity, the CO<sub>2</sub> permeance increased from  $65 \times 10^{-7}$  to  $100 \times 10^{-7}$  mol s<sup>-1</sup> m<sup>-2</sup> Pa<sup>-1</sup> with increasing temperature.

High-silica MFI membranes were also evaluated for CO<sub>2</sub>/H<sub>2</sub> separation, which is critical for syngas purification and H<sub>2</sub> production. The highest CO<sub>2</sub> permeance at the feed pressure of 9 bar was about  $78 \times 10^{-7}$  mol s<sup>-1</sup> m<sup>-2</sup> Pa<sup>-1</sup> at around 300 K, which is one or two order of magnitude higher than those reported previously in the literature. By decreasing the temperature, separation factor reached its highest value of 165 at 235 K.

In summary, zeolite membranes show great potential for CO<sub>2</sub> separation from industrial gases, in particular for CO<sub>2</sub> removal from synthesis gas. For the CO<sub>2</sub>/CH<sub>4</sub> separation the selectivity of the MFI membranes should be improved or other frameworks relying on molecular sieving e.g. the CHA framework should be explored.

Keywords: MFI zeolite, Membrane, CO<sub>2</sub>/CH<sub>4</sub> separation, Si/Al ratio

## Acknowledgements

First of all, I would like to thank my supervisor, Professor Mattias Grahm for all your guidance and support during this work. Further, the head of the chemical technology group, Professor Jonas Hedlund is acknowledged for giving me the opportunity to work within this research group.

I would like to thank Dr. Danil Korelskiy; my assistant supervisor, for his support and fruitful discussions during this project and for encouraging my ideas.

I thank Dr. Liang Yu for your constant enthusiasm. I really enjoyed working with you though it was short.

Special thanks to Shahab, Lindsay, Tommy, Simon, Sadegh, Farshid for cheering me up. It is really fun being with you!

Abrar, Pengcheng, Farrokh and all my former and current colleagues in Chemical technology group, I miss having “*Fika*” with you!

The Swedish Research Council Formas, the County Administrative Board - Länsstyrelsen i Norrbotten and Bio4Energy are gratefully acknowledged for their financial support.

پدر و مادر عزیزم که پشتیبانی و محبتشان پایانی ندارد.

My siblings, Leila, Reza and Sheedeh, Thanks for giving me the confidence to pursue my dreams!

Last but not least, I wish to thank my husband, Babak for always being there for me and for supporting me. You mean the world to me!

*Shahpar Fouladvand,  
November 2016.*



# List of Papers

This thesis is based on the following three papers:

**I. CO<sub>2</sub>/CH<sub>4</sub> separation by highly permeable H-ZSM-5 membranes**

Shahpar Fouladvand, Danil Korelskiy, Liang Yu, Jonas Hedlund and Mattias Grahn.

*To be submitted*

**II. Ultra-thin MFI membranes with different Si/Al ratios for CO<sub>2</sub>/CH<sub>4</sub> separation**

Liang Yu, Shahpar Fouladvand and Jonas Hedlund

*Manuscript*

**III. Efficient ceramic zeolite membranes for CO<sub>2</sub>/H<sub>2</sub> separation**

Danil Korelskiy, Pengcheng Ye, Shahpar Fouladvand, Somayeh Karimi, Erik Sjöberg, Jonas Hedlund

*Journal of Materials Chemistry A*, 3 (2015) 12500-12506

## Conferences contributions

### I. High Performance MFI Membranes for Efficient CO<sub>2</sub> Removal

Danil Korelskiy, Pengcheng Ye, Shahpar Fouladvand, Somayeh Karimi and Jonas Hedlund

*Accepted for Oral Presentation at the International Symposium on Zeolite and Microporous Crystals 2015, Sapporo, Japan*

### II. Zeolite membranes for efficient upgrading of biogas

Shahpar Fouladvand, Danil Korelskiy, Jonas Hedlund, Mattias Grahm

*Accepted for Poster Presentation at the International Symposium on Zeolite and Microporous Crystals 2015, Sapporo, Japan*

### III. Ultra-thin MFI Zeolite Membranes for Efficient Gas Separation

Jonas Hedlund, Danil Korelskiy, Han Zhou, Liang Yu, Simon Barnes, Pengcheng Ye, Shahpar Fouladvand, Mattias Grahm

*Accepted for Oral Presentation at the 18th International Zeolite Conference IZC18, June 2016, Rio de Janeiro, Brazil*

# Content

<b>Abstract.....</b>	<b>I</b>
<b>Acknowledgements .....</b>	<b>III</b>
<b>List of Papers.....</b>	<b>V</b>
<b>Conferences contributions.....</b>	<b>VI</b>
<b>Content.....</b>	<b>VII</b>
<b>Introduction.....</b>	<b>1</b>
Background.....	1
Scope of the work .....	12
<b>Experimental .....</b>	<b>15</b>
Membrane preparation.....	15
Characterization.....	16
Si/Al ratio measurement of the membranes .....	16
Scanning Electron Microscopy.....	16
Permporometry .....	16
Permeation measurements .....	17
<b>Results and discussion .....</b>	<b>19</b>
Si/Al ratio .....	19
SEM investigation .....	19
Assessment of membrane quality by Permporometry .....	22
Single gas permeance and separation measurements .....	23
Effect of Si/Al ratio on the separation performance of MFI membranes .....	27
CO <sub>2</sub> /H <sub>2</sub> separation.....	29
Cost estimation .....	30
<b>Conclusions .....</b>	<b>33</b>
<b>Future work.....</b>	<b>35</b>
<b>References .....</b>	<b>37</b>



# Introduction

## Background

Nowadays, there is a global trend towards finding renewable sources of energy and raw materials for chemicals [1] and to reduce emissions of greenhouse gases. Biogas is widely regarded as a good alternative vehicle fuel [2] and a versatile renewable source of energy which can be considered as a sustainable substitute for natural gas but it can also be used in industrial processes and as raw material in chemical industry [3]. Biogas may be produced from anaerobic digestion of organic substrates such as manure, sewage sludge and organic waste, etc and also by anaerobic degradation of organic substances in landfills (landfill gas) [3]. According to the EU28, energy production from biogas within the EU was estimated to be 141 TWh in 2012 [4] with Germany being the country in the world producing the largest amount of biogas [5]. The composition of raw biogas varies from source to source, but the main components are methane and carbon dioxide [6]. Carbon dioxide is also a common impurity in natural gas. Whether the carbon dioxide has to be reduced or removed or not from biogas or natural gas depends on the targeted application. As CO<sub>2</sub> is one of the main impurities in biogas and in many natural gas resources, it has to be reduced or removed since it lowers the calorific value of the gas and it may also cause corrosion in pipes, fittings etc [6]. The energy content in the gas is proportional to the methane content. If the gas is to be used as fuel, the Wobbe index is often used as a measure of the energy content, or

quality, of the gas [7, 8]. Figure 1 shows how the Wobbe index and the relative density of biogas varies with the methane content in the gas [6].

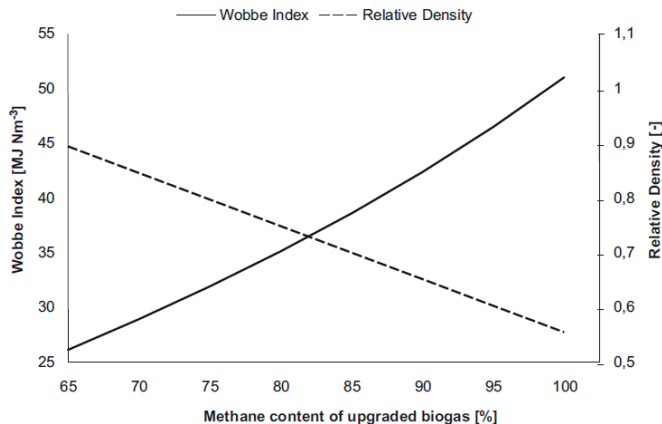


Figure 1. Wobbe index and relative density of upgraded biogas versus methane content [6].

In this study, biogas upgrading is described as removal of CO<sub>2</sub> from biogas. There are several technologies for upgrading biogas. Some of them are commercialized and others are yet under development at pilot or demonstration plants [3]. Many of the technologies used for upgrading of biogas have been adopted from the very similar process of removal of carbon dioxide from natural gas. The main differences between the two processes is that the carbon dioxide content in natural gas may vary more and that upgrading of natural gas usually is operated in much larger scale than upgrading of biogas. Some of the common techniques for upgrading of biogas include: amine scrubbing, water scrubbing, pressure swing adsorption (PSA), membrane separation and physical scrubbing with organic solvents [2]. Cryogenic separation, in situ methane enrichment and ecological lung [3] are examples of new technologies under development. Today's dominant market technologies for upgrading biogas are water scrubbing, pressure swing adsorption and amine scrubbing, with amine scrubbing being less common compared to the other two [2]. Investment and operation cost, energy demand, gas purity and methane slip are among the critical factors that have to be considered when choosing the most suitable technology [2]. A brief description of the different upgrading technologies is listed in Table 1. Amine absorption usually shows very high selectivities with 99.8% gas purity (CH<sub>4</sub> content) whereas other systems are capable of reaching 98-99% purity. The energy demand for all the technologies is about the same. At

high output, the investment cost is almost the same for all systems, but in small to mid-scale the membrane technology has lower and amine system higher investment cost [2]. Methane slip in PSA is quite high of about 1.8-2%, water scrubbing has a methane slip of about 1% and amine scrubbing has low slip of about 0.1%, but another 1-4% methane is used for heat production to regenerate the amine solution which makes total methane loss of about 2-5% [9]. Organic physical scrubbers has the highest methane slip, this methane is used for heat production to provide the required energy for desorption [2]. Nowadays, developments in membrane material and processes enable them to minimize the methane slip to below 1% [2]. Membrane process presents other advantages over the other technologies which are particularly important for small scale operations. Safety and ease of operation, simple maintenance and operation without hazardous chemicals are the most important advantages of membranes [10] especially for plants for upgrading biogas since they are usually in quite small scale e.g. at farms and not operated by specially trained personnel [11].

Table 1. Brief description of different commercialized biogas upgrading technologies[12].

Biogas upgrading technology	Description
Water scrubbing	Dissolving of CO <sub>2</sub> in water
Pressure swing adsorption	Adsorption on adsorbent materials
Amine absorption	Dissolving CO <sub>2</sub> in a amine solution, associated with chemical reaction
Membrane separation	Permeation of the selective compound through membrane
Physical solvent scrubbing	Absorption process without chemical reaction

Natural gas is both an important source of energy and important raw material for the chemical industry, due to its high hydrogen(H)/carbon(C) –ratio. Due to recent concerns regarding emission of greenhouse gases, like CO<sub>2</sub>, to the atmosphere being coupled to climate change, the favourable H/C ratio of methane in natural gas has increased the interest of using natural gas as a fuel for heating or power production. Natural gas (NG) may be classified as

associated NG or non-associated NG. Associated NG is obtained as a by-product to the production of crude oil. As a consequence, associated natural gas typically contains hydrocarbons in the C2-C7-range in significant amounts, whereas the CO<sub>2</sub> content is often rather low. Non-associated natural gas, on the other hand, is produced from reserves developed primarily for natural gas production with typically only minor fractions of other hydrocarbons than methane in the gas. Natural gas is often produced in remote areas and is then typically transported long distances by pipelines. It is therefore essential that the natural gas meet the pipeline specification, which is a number of criteria specifying e.g. how much impurities the gas may contain. The carbon dioxide levels should for instance be low to reduce the risk of corrosion and to reduce the cost for transporting an inert gas long distances in the pipeline. The content of hydrocarbons larger than methane also needs to be controlled to avoid the risk of condensation of these in the compressor or in the pipeline. The global consumption of natural gas is about 95 trillion scf (standard cubic feet) per year [9] so upgrading of natural gas is by far the largest industrial gas separation process. Membrane separation, chemical (amine absorption) and physical (e.g. Rectisol or Selexol) absorption, adsorption (e.g. on zeolite NaX or on activated carbon), polymeric membranes and cryogenic separation are available techniques for upgrading natural gas, with amine absorption being the dominant technique [9, 13]. Upgrading of natural gas by membrane technology has been identified as a promising technology with high potential for further improvement by further developing the membrane materials and process design [9, 14].

Synthesis gas, also known as syngas, is an important intermediate in the chemical industry. It may be produced by gasification of e.g. coal, heavy oils or biomass, another option is by steam reforming of methane or light nafta [15]. Synthesis gas mainly contains of CO, CO<sub>2</sub>, H<sub>2</sub>, CH<sub>4</sub> and water, the composition depends on the composition of the raw material used and the processing conditions. Syngas can be used for production of e.g. ammonia (hydrogen production is maximized), hydrogen, methanol or higher hydrocarbons useful as liquid fuels via the Fischer Tropsch process. The extent to which the synthesis gas needs to be upgraded depends on the application, but for most applications, carbon dioxide has to be removed from the syngas. For ammonia synthesis and H<sub>2</sub> production virtually all CO<sub>2</sub> and CO need to be removed as both are poisons to the ammonia catalyst. On the other hand, for methanol synthesis it is

beneficial to have some CO<sub>2</sub> still in the syngas, such that the composition of the gas, expressed as the stoichiometric ratio (in moles), (H<sub>2</sub>-CO<sub>2</sub>) / (CO+CO<sub>2</sub>) is close to 2 [16]. If the syngas is produced via gasification of coal or biomass, the syngas often contains more CO<sub>2</sub> than desired and the excess should be removed. If the syngas is produced via steam reforming of methane, removal of CO<sub>2</sub> may not be necessary. The technologies used for CO<sub>2</sub> removal from synthesis gas is very similar to those used for upgrading natural gas mentioned above.

Table 2 briefly shows the general composition of biogas, natural and syngas.

Table 2. General composition of biogas, natural gas and syngas (vol%) [3, 17, 18].

	Biogas	Associated natural gas	Syngas
CH <sub>4</sub>	65	84.6	few percent
CO			40
CO <sub>2</sub>	35	≤5	15
H <sub>2</sub> S	0-4000 ppm	≤5	Trace
H <sub>2</sub>	0	Trace	30
H <sub>2</sub> O	trace		25
N <sub>2</sub>	~0.2	≤10	Trace
Other hydrocarbons	0	≥13	

Membranes are selective barriers that control the rate of transport of different chemical species through a material. It can be permeable, semi-permeable and impermeable to various species. The major industrial application of membranes is in gas separation [19], however membranes are also used for other applications e.g. desalination of water by forward or reverse osmosis. In gas separation process by membranes, one component preferentially permeate through the membrane and the other components will permeate at slower rate or not at all [20]. Figure 2 shows a schematic figure of a simple membrane separation process. The stream fed to the membrane is referred to as feed. Permeate is the fraction of the feed passing through the membrane while the retentate is the stream rejected by the membrane [19, 21].

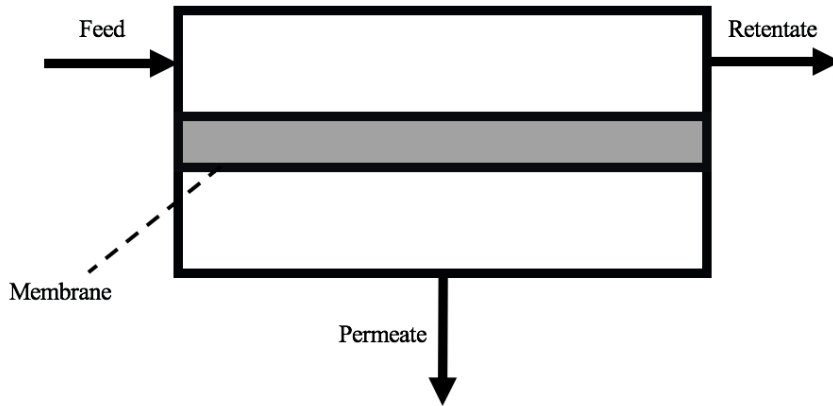


Figure 2. Schematic diagram of membrane separation process.

To facilitate transport through the membrane, a driving force has to be applied. Pressure, temperature, concentration and electrical potential gradient are common driving forces for transport through membranes [19]. For gas separations, the driving force is usually expressed as a partial pressure difference with a transport from the high pressure, feed side, to the low pressure permeate side. An inert gas, e.g., nitrogen, referred to as the sweep gas can also be fed to the permeate side in order to reduce the permeate concentration on the permeate side, thereby increasing the concentration gradient. However most industrial gas separations usually operate without sweep gas.

Pressure ratio; one of the important factors that control the membrane's performance, is defined as the ratio of feed pressure to permeate pressure across the membrane [19]. Consequently, separation can never exceed the pressure ratio  $p_0/p_l \geq n_{i_0}/n_{i_l}$ . Where  $n_{i_0}$  and  $n_{i_l}$  are the feed and permeate concentrations of component  $i$ . Depending on the properties of the membrane material and the operating conditions, the separation may be limited by membrane-selectivity or pressure ratio or a combination of both. In case of having much greater intrinsic selectivity of the membrane material than the pressure ratio ( $\alpha \gg p_0/p_l$ ), due to practical limits in increasing the pressure ratio which requires either deep vacuum on the permeate side or compressing of

the gas on the feed side, the benefit of highly selective membrane is often less than expected [19].

The transport of species through the membrane is often expressed as the flux through the membrane. Flux is defined as the permeate flow per unit area per unit time, with typical units  $mol\ m^{-2}\ s^{-1}$ . To be able to compare the performance of different membranes where different driving forces have been used, it is common to also report the permeance, which is defined as the flux of a component per unit driving force (partial pressure gradient):

$$\Pi_i = \frac{J_i}{\Delta P_i} (mol\ m^{-2}\ s^{-1}\ Pa^{-1}) \quad (1)$$

Where  $\Pi_i$  is the permeance of component  $i$ ,  $J_i$  is the flux and  $\Delta P_i$  is partial pressure gradient of component  $i$  across the membrane. By taking the ratio of the permeances for two gases, the permselectivity of the membrane may be determined:

$$\alpha_{i,j}^{Perm} = \frac{\Pi_i}{\Pi_j} \quad (2)$$

If the permeances were determined by experiments where one gas at a time was fed to the membrane (pure-gas permeances), the selectivity is denoted ideal permselectivity. On the other hand, if the permeances were obtained from a separation experiment where a gas mixture is fed to the membrane (mixed-gas permeances), the selectivity is just denoted permselectivity (or sometimes selectivity for short). Another way of reporting the separation performance of a membrane is to report the separation factor which is defined as:

$$\beta = \frac{(n_i/n_j)_{permeate}}{(n_i/n_j)_{feed}} \quad (3)$$

$n_i$  and  $n_j$  are the concentration of components ( $i$  or  $j$ ) on the permeate and feed side, respectively.

Ideally a membrane should show both high flux and selectivity to minimize both capital and operation costs [19, 20]. High flux makes it possible to process a

certain quantity of gas with a low membrane area which is reducing capital costs and a selective membrane may facilitate the use of a simple process design with small losses, slip, of the valuable components [22].

Membranes may be classified as either isotropic or anisotropic. Isotropic membranes have uniform composition and structure all through whereas anisotropic membranes are composed of layers with different structures. For example, a thin selective layer on top of a thicker support layer giving mechanical strength to the membrane. They can also be classified as porous, nonporous (dense) and electrically charged membranes [19]. This study focuses on microporous membranes. The pores in microporous membranes are extremely small not exceeding 2 nm. Once a molecule or particle reaches a pore, if the particle is smaller than the pore, it can permeate through the membrane, otherwise the particle will be rejected.

Membranes can be manufactured from both organic and inorganic materials. The majority of the commercialized membranes are polymer-based. However, recently inorganic membranes have attracted a lot of attention due to their high thermal and chemical stability [19] together with good selectivity and high permeability. For instance, H-ZSM-5; a crystalline zeolite membrane, shows both higher permeance and gas separation selectivity compared to polymer membranes [23].

Zeolites are microporous crystalline aluminosilicates with a three dimensional framework structure created by  $\text{SiO}_4$  tetrahedra as primary building units. Upon Al incorporation into the silica framework,  $\text{Al}^{3+}$  replaces the  $\text{Si}^{4+}$  which makes the framework negatively charged. This charge will be counterbalanced by an extra-framework cation which gives zeolites ion exchangeability. Today, more than 200 different zeolite frameworks topologies have been approved by the structure commission of the International Zeolite Association [24]. Each framework is identified by a three-letter code irrespective of composition. The final framework of the zeolites is made of collection of the secondary building units which are the assembled form of primary units (polyhedral building units such as cubes, octahedral and etc.). The definition of “zeolite” has changed over the last decade which also includes non-aluminosilicate compositions, so the structure is formed by  $\text{TO}_4$  and T-elements can be P, Ga, B, etc. other than Si

and Al [25]. Zeolite are special due to their interesting properties such as: well-defined microporous structure with uniform pore dimensions (molecular sieving), the ion-exchange properties (ion-exchange reactions), shape selective acid catalysts and high thermal stability [25]. Today, the largest application for zeolites, in terms of volume, is in detergents (70%) as builder followed by catalysis with 9% of the total consumption [25].

In this work, the MFI framework is investigated, MFI zeolite has a medium pore size of  $\sim 0.55$  nm (ten member-ring pore) with the pore system composed of both straight and intersecting zigzag channels (3D channels). Figure 3 shows the topology of MFI zeolite. S, Z and I are Straight, Zigzag channels and Intersections [26].

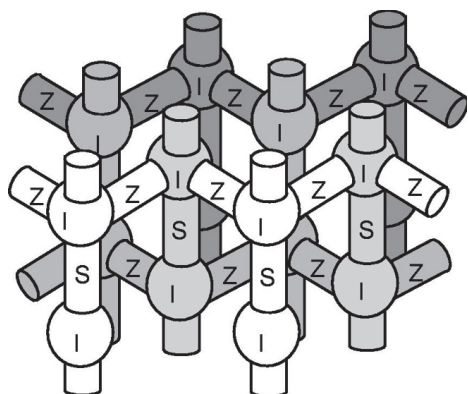


Figure 3. MFI zeolite pore topology [26].

Zeolite MFI exists in two forms, *i.e.* silicalite-1 and ZSM-5 with the difference being the aluminum content in the framework. Silicalite-1 is the (virtually) Al-free zeolite and ZSM-5 has Si/Al ratio larger than 10 [27]. In other words, MFI zeolites with a Si/Al ratio of 10-200 and higher than 200 are categorized into ZSM-5 and silicalite-1, respectively [28]. Apart from concentration of charge balancing cations and ion-exchange capability, which are directly proportional to the aluminum content of the framework, the aluminum content also affects other properties of the zeolite. The higher the aluminum content, the more polar, and hence hydrophilic the structure becomes. Consequently, all silica zeolites are the least hydrophilic, *i.e.* the most hydrophobic [25]. High aluminum content

also decreases the thermal stability and increase the number of acid sites in zeolites [25, 29].

Because of their well-defined microporous structure, the ability to tailor the polarity of the framework and high stability, it has been realized that zeolite membranes may potentially excel over other membrane materials in many applications. Most of the work on zeolite membranes have been devoted to the MFI and LTA frameworks, where the former has been extensively investigated for various gas separations whereas the latter framework has been mainly investigated for dehydration of organics e.g. ethanol.

As mentioned above, in order to make membranes industrially feasible, the membranes should have high fluxes and sufficient selectivities. Therefore, the membranes have to be very thin ( $< 1\ \mu\text{m}$ ) and without defects (pores larger than the zeolite pores) to fulfill these requirements. Different types of flow-through defects may exist in zeolite membranes such as open grain boundaries - a common type of defect, pinholes and cracks [30, 31]. The presence of defects can dramatically decrease the selectivity of the membrane. Consequently, characterization of the size and amount of defects in membranes is of great importance [32]. Our research group has significantly developed a non-destructive technique referred to as permoporometry to enable careful characterization of both micropore and mesopore defects in ultra-thin high-flux MFI membranes [33, 34]. In this technique, the permeance of a non-adsorbing gas, e.g., helium is measured as a function of the relative pressure of an adsorbing gas, e.g., *n*-hexane in the feed. The higher the concentration of adsorbate added to the feed, larger and larger pores and defects will be blocked by capillary condensation. The adsorbate concentration is increased stepwise during the experiment, thus reducing the He gas permeance gradually larger and larger pores are blocked. Knowing the concentration of the adsorbate in the feed, both the pore (defect) size and the amount (relative area) of them can be estimated by Horváth-Kawazoe (micropores) and Kelvin equations (mesopores) [35].

The separation mechanism for zeolite membranes can be classified in three groups: molecular sieving, selective adsorption and diffusion. Figure 4 shows the three separation mechanisms schematically. Separation by zeolite

membranes is usually governed by a combination of these mechanisms. If the separation is governed by adsorption, one or several components travel across the membrane while the non-adsorbing components are rejected. In diffusion-controlled separation, components with higher diffusivity in the membrane pores diffuse faster and preferentially permeate the membrane. In molecular-sieving, the molecules smaller than the pores can permeate through the membrane, whereas molecules larger than the pores will be hindered. H<sub>2</sub>, CO<sub>2</sub> and CH<sub>4</sub> have smaller kinetic diameter than the pores of zeolite MFI, and therefore both adsorption and diffusion play important roles in the transport through the membrane in this study.

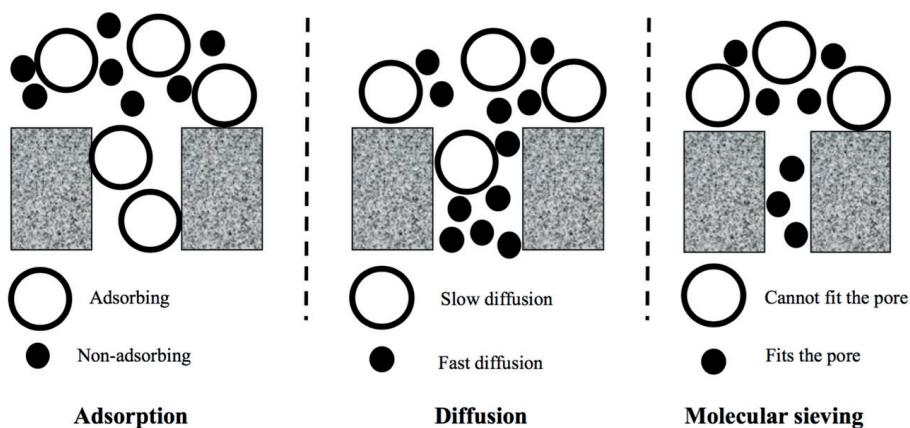


Figure 4. Separation mechanisms in zeolite membranes.

As mentioned above, zeolite membranes show great potential for being used for gas separations. CO<sub>2</sub> separation from CH<sub>4</sub> and H<sub>2</sub> was studied in the present work by very thin MFI zeolite membranes. Nowadays, membranes are considered to be one of most promising CO<sub>2</sub> separation technologies [23]. Commercial membranes often have a separation factor of about 20 for CO<sub>2</sub>/CH<sub>4</sub> separation in natural gas. The commercial cellulose acetate membranes which are most widely used and tested membrane for natural gas sweetening typically have CO<sub>2</sub>/CH<sub>4</sub> separation selectivity of 10-20 and CO<sub>2</sub> permeance of 60-110 GPU [9]. Sandström et al. also reported CO<sub>2</sub>/CH<sub>4</sub> separation factor of 4.5 with high CO<sub>2</sub> permeance of about  $45 \times 10^{-7} \text{ mol s}^{-1} \text{ m}^{-2} \text{ Pa}^{-1}$  at 277 K. They also reported the upward trend of separation factor with decreasing temperature [36].

Kosinov et al. reported the CO<sub>2</sub>/CH<sub>4</sub> selectivity of 42 with the low CO<sub>2</sub> permeance of  $3 \times 10^{-7} \text{ mol m}^{-2} \text{ s}^{-1} \text{ Pa}^{-1}$  for CHA (SSZ-13) membrane at pressure of 6 bar and the temperature of 293 K [37]. Tian et al. have synthesized a SAPO-34 membrane with the room temperature separation selectivity of 9 and the CO<sub>2</sub> permeance of  $25 \times 10^{-7} \text{ mol m}^{-2} \text{ s}^{-1} \text{ Pa}^{-1}$  [38]. Van den Bergh et al. also reported a CO<sub>2</sub>/CH<sub>4</sub> selectivity higher than 3000 at 225 K and a total feed pressure of 101 kPa for a DDR membrane. However, the small pores also contribute to the resulting low CO<sub>2</sub> permeance of about  $1.0 \times 10^{-7} \text{ mol m}^{-2} \text{ s}^{-1} \text{ Pa}^{-1}$  [39]. Recently, Yang et al. reported the CO<sub>2</sub>/CH<sub>4</sub> selectivity of DDR of 92 for a feed mixture of 90% CO<sub>2</sub> and 10% CH<sub>4</sub> with the low CO<sub>2</sub> permeance of  $1.8 \times 10^{-7} \text{ mol m}^{-2} \text{ s}^{-1} \text{ Pa}^{-1}$  at the pressure of 2 bar and the temperature of 297 K [40]. So far polymer membranes have been the most of commercially successful membranes. Today's best polymeric membranes have shown CO<sub>2</sub>/H<sub>2</sub> separation selectivity of 10-12 with a CO<sub>2</sub> permeance of *ca.*  $2 \times 10^{-7} \text{ mol s}^{-1} \text{ m}^{-2} \text{ Pa}^{-1}$  at room temperature [41]. Such a low permeance needs to be compensated by quite large membrane area.

## Scope of the work

The main goals of the present work were to test the effect of temperature and Si/Al ratio (polarity) on the separation performance of zeolite MFI membranes for the CO<sub>2</sub>/CH<sub>4</sub> (biogas and natural gas) separation and to identify the limiting factors for obtaining higher selectivity and how to reduce their negative effect. Another goal was to study the effect of temperature on the CO<sub>2</sub>/H<sub>2</sub> separation (syngas) for MFI membranes at high feed pressures.





## Experimental

In this section the experimental methods used in the work are summarized, the reader should consult the appended papers for details.

### Membrane preparation

Thin MFI membranes with a film thickness of *ca.* 0.5-1  $\mu\text{m}$  were grown on porous, graded asymmetric  $\alpha$ -alumina support discs (Fraunhofer IKTS, Germany) with a diameter and thickness of 25 and 3 mm, respectively. The alumina supports are composed of two distinct layers; a thin top layer with a thickness of 30  $\mu\text{m}$  and a pore size of 100 nm, and a thicker bottom layer of 3 mm in thickness with a pore size of 3  $\mu\text{m}$ . The support is used to provide mechanical strength to the membrane.

The procedure for preparation of thin MFI membranes (paper I and III) have been described in detail previously by Hedlund et al. and will only be described here briefly [33]. The masked (performed to avoid zeolite growing in the pores of the support) supports were treated with cationic polymer to facilitate the deposition of a dense monolayer of colloidal MFI seed crystals (50 nm) on the support surface. Subsequently, the seed layer was grown into a continuous layer by hydrothermal synthesis. Different masking technique was used for membranes in paper II. For all the membranes, the molar composition of the synthesis solution was altered to arrive at zeolite films with different polarity. For preparing a zeolite membrane with low aluminum content (papers I, II and III), a synthesis mixture free from aluminum was used, the synthesis mixture had the following composition: 3 TPAOH: 25  $\text{SiO}_2$ : 1450  $\text{H}_2\text{O}$ : 100 EtOH. For

preparing membranes with Si/Al=50, aluminum isopropoxide ( $\geq 98.0\%$ , Aldrich) was used as aluminum source. Sodium hydroxide (NaOH,  $\geq 99.0$ , Merk) was also added in order to increase the basicity of the solution the molar composition of the synthesis mixture was 3TPAOH:  $0.25\text{Al}_2\text{O}_3$ :  $\text{Na}_2\text{O}$ :  $25\text{SiO}_2$ :  $1600\text{H}_2\text{O}$ :  $100\text{EtOH}$  and the zeolite film was grown at 373 K for 22 h under reflux. A synthesis solution having a molar composition of 3TPAOH:  $0.5\text{Al}_2\text{O}_3$ :  $\text{Na}_2\text{O}$ :  $25\text{SiO}_2$ :  $1600\text{H}_2\text{O}$ :  $100\text{EtOH}$  was used for preparation of the membrane with Si/Al ratio of 25. The hydrothermal treatments for the membranes with low aluminum content in paper I and II were at 361 K for 72 h and 55 h, respectively. After synthesis, all the membranes were rinsed and calcined at 773 K for 6 h.

## **Characterization**

### **Si/Al ratio measurement of the membranes**

XPS (X-Ray Photoelectron Spectroscopy) was used to determine the Si/Al ratio of the MFI membranes. The XPS spectra were collected with a Kratos Axis Ultra DLD spectrometer using a monochromated Al K $\alpha$  source operated at 120 W. An analyser pass energy of 160 eV for acquiring wide spectra and a pass energy of 20 eV for individual photoelectron lines were used. The surface potential was stabilized by the spectrometer charge neutralization system. The binding energy (BE) scale was referenced to the C 1s line of aliphatic carbon, set at 285.0 eV. Processing of the spectra was accomplished with the Kratos software.

### **Scanning Electron Microscopy**

SEM images were recorded using an FEI Magellan 400 field emission XHR-SEM to study the morphology and thickness of the membranes. The samples were not coated prior to the investigations.

### **Permporometry**

*n*-hexane/helium adsorption-branch permporometry [33] analysis was performed to assess the quality of the membranes by measuring the size distribution of flow-through defects in the membranes. The method and data evaluation are

described in detail in a previous publication [34]. In short, the membrane was first mounted in a stainless steel Wicke–Kallenbach cell sealed with graphite gaskets and thereafter the membrane was dried at 573 K for 6 h in a helium flow (99.999%, AGA). The pressure difference across the membrane was 1 bar with an atmospheric permeate pressure. The relative pressure of *n*-hexane was increased gradually and the system was allowed to equilibrate at each measuring point. The width of defects smaller and larger than 2 nm was estimated by the Horvath-Kawazoe (H-K) equation and the Kelvin equation, respectively. The defects area was calculated from the measured helium molar flow and the corresponding helium molar flux through the defects estimated from Fick's law. The defect distribution was evaluated in terms of relative areas of defects (area of defects divided by the total membrane area).

## **Permeation measurements**

### *Single gas permeation experiments*

After the permoporometry measurements, the membrane retained in the cell was again dried at 573 K for 6 h at a heating rate of 1 °C/min under helium flow. Afterwards, single gas permeances were measured in the defined temperature range. During the single gas experiment, the feed pressure was kept at 4.5 bar whereas atmospheric pressure was used on the permeate side.

### *Separation experiments*

The membrane was kept in the stainless steel cell and dried at 573 K for 6 hours in a helium flow prior to the separation experiments. Digital mass flow controllers were used to adjust the composition of gases with the defined flow rate. The pressure on the feed- and permeate side was 9 and 1 bar respectively adjusted by a back pressure regulator. A mass spectrometer (GAM400, InProcess Instrument) was used to analyze the composition of the permeate stream. The permeate volumetric flow rate was measured by a drum type gas meter (TG 5, Ritter Apparatebau GmbH). The separation experiment was carried out in the same temperature range as used for the single gas permeation experiments. During the experiment the temperature in the membrane cell was monitored by a type K thermocouple connected to the feed side of the membrane.



## Results and discussion

### Si/Al ratio

The Si/Al ratios of the membranes were measured by X-Ray Photoelectron Spectroscopy (XPS). The measured Si/Al ratios of the membranes are shown in Table 3.

Table 3. Si/Al ratios of synthesized membranes according to XPS.

Si/Al ratio in synthesis solution	Measured Si/Al in membrane
$\infty$	90
50	46
25	21

Table 3 shows the lower Si/Al ratio in the zeolite film compared to the corresponding value in the synthesis solution at the start of the synthesis. The Si/Al ratio of the initial synthesis solution is generally higher than what is measured in the zeolite film. This can be attributed to aluminum leaching from the support during synthesis that is then incorporated in the film and/or that the Si/Al ratio becomes somewhat lower in the crystallized material than in the original synthesis solution [42].

### SEM investigation

Cross-section and top-view SEM images of the as-synthesized MFI membranes with different Si/Al ratios are shown in Figures 5-8. The membrane used in Paper I appears to have a thickness of about 450 nm, see Figure 5. Further, the

film is composed of well-intergrown crystals, free from large defects ( $> 5\text{nm}$ ) and no invasion of zeolite phase into the pores of the support was detected.

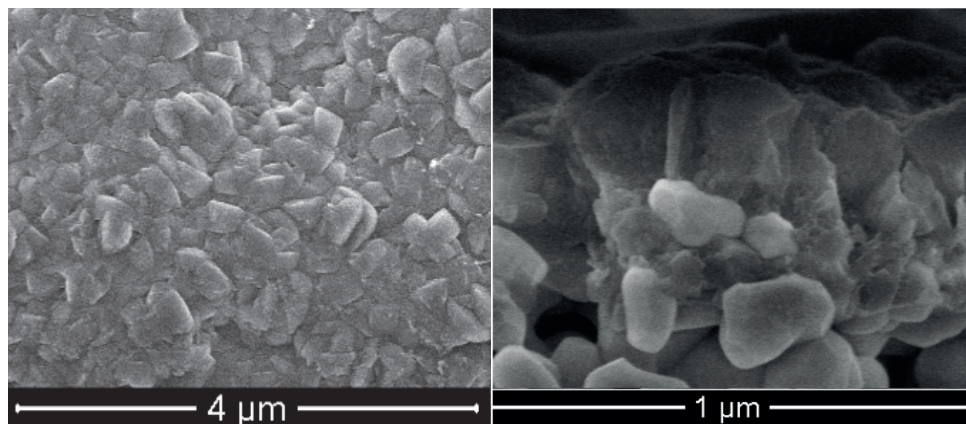


Figure 5. Top-view (left) and cross-section (right) SEM images of high silica MFI membrane (paper I).

Paper II deals with the effect of the aluminum content on the performance of MFI membranes for  $\text{CO}_2/\text{CH}_4$  separation. The film thickness in membranes with Si/Al ratios 90 and 46 are about 350 nm and the supports are fully open indicating that no invasion occurred, see Figures 6 and 7 respectively. The membrane with Si/Al ratio of 21 was thicker with a film thickness of about 750 nm which is about twice thicker than the previous two membranes with Si/Al ratios of 90 and 46. The zeolite crystals were also larger with well-developed grain boundaries, resulting in the presence of pinholes in the film, see Figure 8.

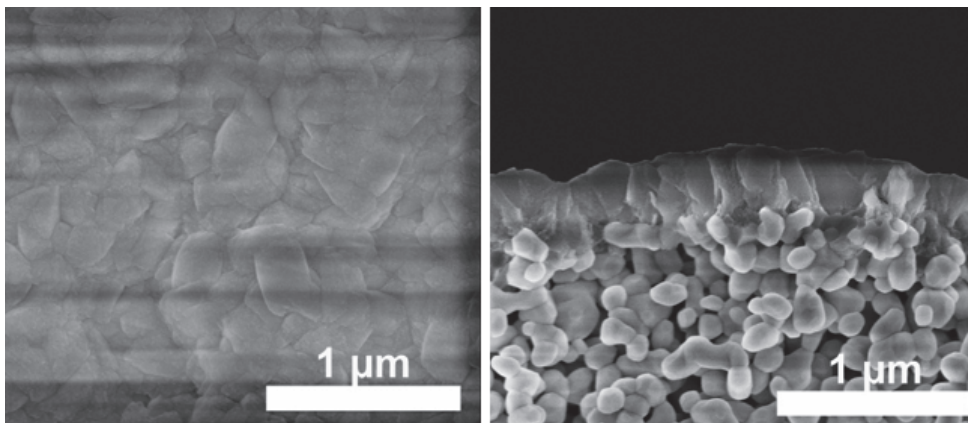


Figure 6. Top view (left) and cross-section (right) SEM images of MFI membrane with Si/Al= 90.

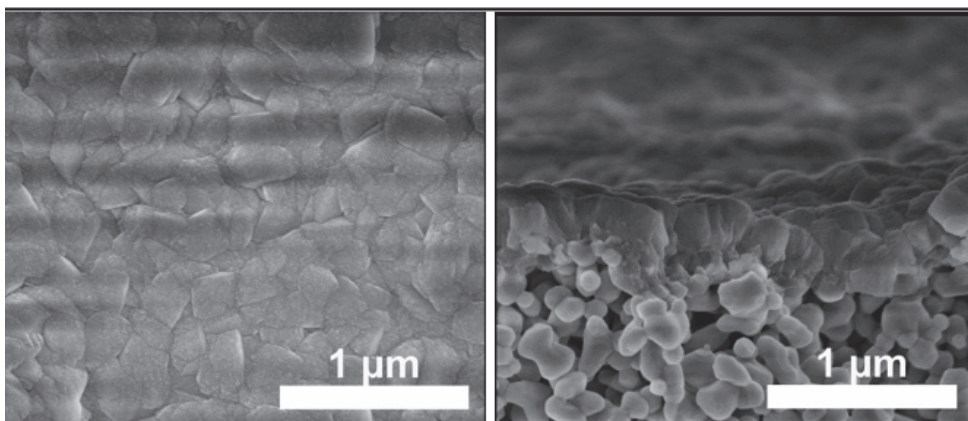


Figure 7. Top view (left) and cross-section (right) SEM images of the MFI membrane with Si/Al= 46.

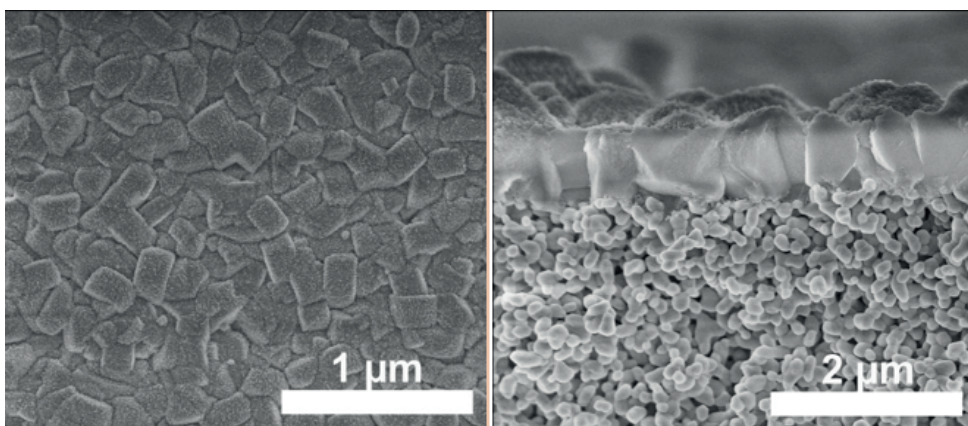


Figure 8. Top view (left) and cross-section (right) SEM images of the MFI membrane with Si/Al= 21.

## Assessment of membrane quality by Permporometry

The permporometry patterns for the membranes used in Papers I & III show that the membranes are of high quality. In Paper I, the high initial (no *n*-hexane in the feed) He permeance of  $53 \times 10^{-7} \text{ mol s}^{-1} \text{ m}^{-2} \text{ Pa}^{-1}$  shows that the zeolite pores are open and rather permeable. The relative area of defects was estimated to be 0.001% where about 77.2% of the defects are micropore defects ( $< 2\text{nm}$ ), most likely open grain boundaries. Nearly no larger defects ( $> 5\text{nm}$ ) were detected, which is in line with the SEM data.

Permporometry patterns for the three membranes with different Si/Al ratios used in Paper II are shown in Figure 9. For the membranes with Si/Al ratios of 90 and 46 the He permeance decreased dramatically after introducing *n*-hexane, indicating the presence of mostly micropores and no large defects, these membranes may thus be considered having high quality. The third membrane, with a Si/Al ratio of 21, has reasonably good quality with some larger defects also present as indicated by SEM images.

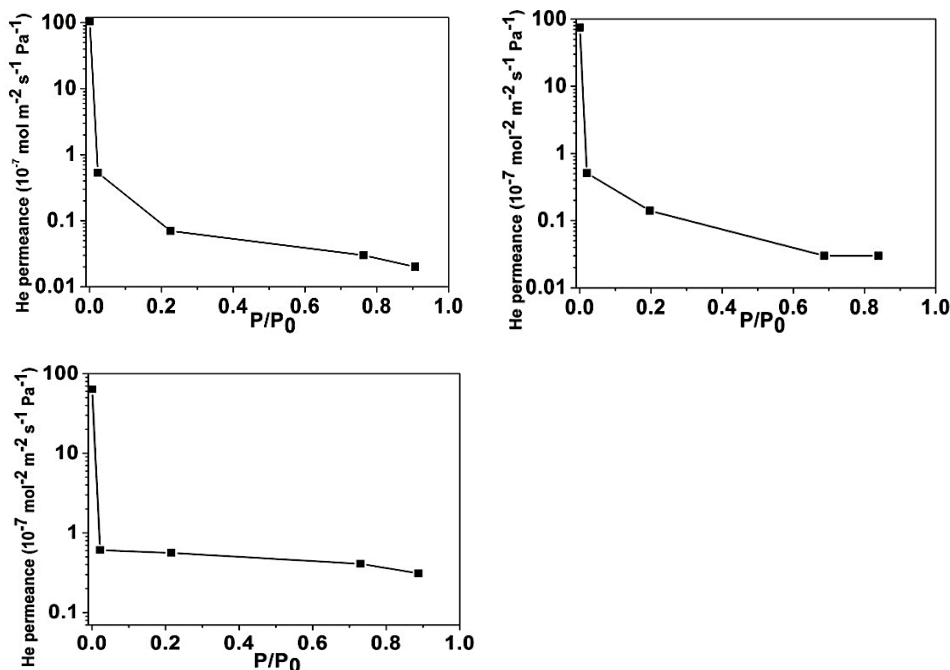


Figure 9. Permporometry patterns for MFI membranes with Si/Al of 90 (upper left), 46 (upper right) and 21 (bottom).

## Single gas permeance and separation measurements

Figure 10 shows the single gas permeances of methane and carbon dioxide through a high silica MFI membrane as a function of temperature (Paper I). The  $\text{CH}_4$  single gas permeance was higher than that of  $\text{CO}_2$  in the entire temperature range and increased slightly with decreasing temperature from 290 K to 265 K. When the temperature was decreased further, the permeance was almost constant. On the contrary, the  $\text{CO}_2$  permeance decreased with decreasing temperature in the entire temperature range. To understand this behavior, the driving force, expressed as difference in adsorbed loading, over the zeolite was determined. It was found that the driving force for  $\text{CO}_2$  decreased from 0.31 to 0.095  $\text{mol g}^{-1}$  when the temperature was decreased from 290 K to 250 K, the adsorbed loading on the permeate side increased faster than that on the feed side as the temperature was decreased, resulting in smaller driving force over the film at lower temperatures. Moreover, it is well known that diffusivity decreases with decreasing temperature and with increased adsorbed loading [43]. For  $\text{CH}_4$  on the other hand, the driving force was rather constant varying from *ca.* 0.36  $\text{mol g}^{-1}$  at 250 K and 290 K to 0.39  $\text{mol g}^{-1}$  at 265 K. It should be noted that, the driving forces and diffusivity for  $\text{CH}_4$  is larger than those for  $\text{CO}_2$  in MFI zeolite [44]. The higher diffusivity and driving force therefore explains the higher observed permeance of  $\text{CH}_4$  as compared to  $\text{CO}_2$ . As the activation energy of diffusion and adsorbed loading of methane is lower than the corresponding values for  $\text{CO}_2$ , the permeance of  $\text{CH}_4$  is not affected to the same extent as  $\text{CO}_2$  when the temperature is decreased.

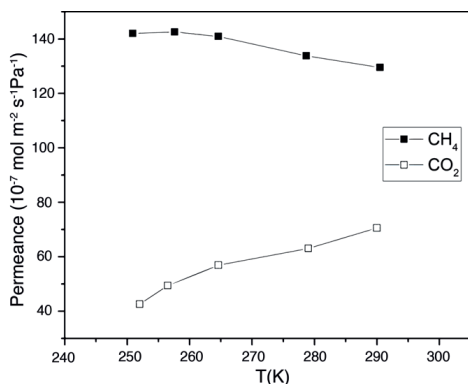


Figure 10. Single gas permeances of  $\text{CH}_4$  and  $\text{CO}_2$  in an MFI membrane as a function of temperature at 4.5 bar feed pressure (Paper I).

Figure 11 shows the CO<sub>2</sub> and CH<sub>4</sub> mixed-gas permeances from the binary mixture (Paper I). The high silica MFI membrane showed a very high CO<sub>2</sub> permeance of  $60 \times 10^{-7} \text{ mol s}^{-1} \text{ m}^{-2} \text{ Pa}^{-1}$  at the lowest temperature of about 245 K and it was even higher at room temperature *viz.* about  $90 \times 10^{-7} \text{ mol s}^{-1} \text{ m}^{-2} \text{ Pa}^{-1}$ . These values are higher than reported previously in the open literature for this separation. For instance, Sandström et al. reported high CO<sub>2</sub> permeance of about  $45 \times 10^{-7} \text{ mol s}^{-1} \text{ m}^{-2} \text{ Pa}^{-1}$  at 10 bar at 277 K for MFI membrane [36]. Kosinov et al. reported a CO<sub>2</sub> permeance of  $3 \times 10^{-7} \text{ mol m}^{-2} \text{ s}^{-1} \text{ Pa}^{-1}$  for a CHA (SSZ-13) at 6 bar feed pressure and a temperature of 293 whereas Tian et al. also reported the CO<sub>2</sub> permeance of  $25 \times 10^{-7} \text{ mol m}^{-2} \text{ s}^{-1} \text{ Pa}^{-1}$  for SAPO-34 membrane at room temperature [37, 38].

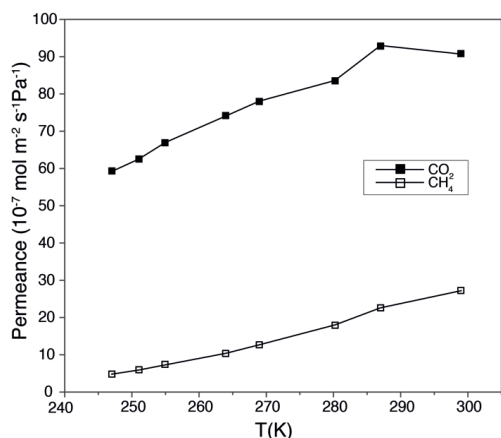


Figure 11. CO<sub>2</sub> and CH<sub>4</sub> permeances of the binary mixture (Paper I).

For high flux membranes, the performance may be affected by external mass transfer limitations (concentration polarization) on the feed side as well as pressure drop over the porous support [45-47]. Both effects may reduce the flux through the membrane and the membrane selectivity. Modeling was performed to investigate if these phenomena had influenced the separation performance. Indeed, the pressure drop over the support was significant, varying from 32 % at 299 K where the flux of carbon dioxide was highest to 17% at the lowest temperature where the flux was also the lowest, see Table 4. Decreasing the thickness of the top layer of the support, which is composed of small pores of about 100 nm in diameter, or increasing the pore size would be a means of reducing the pressure drop over the support. Concentration polarization is often

expressed through the concentration polarization index (CPI), defined as the ratio between the concentration of CO<sub>2</sub> at the membrane surface to the concentration of CO<sub>2</sub> in the gas bulk on the feed side,  $C_{\text{CO}_2, \text{mem}}/C_{\text{CO}_2, \text{bulk}}$ . These ratios were about 0.95, i.e. close to unity, at all temperatures studied, see Table 4, indicating that the concentration polarization on the feed side only had a very small effect on the performance of the membranes.

Further, the intrinsic permselectivity of the zeolite film was estimated by calculating film permeances using the partial pressures on each side of the zeolite film obtained from the CPI and pressure drop calculations. After removing the adverse influence of pressure drop over the support, it was found that the intrinsic permselectivity of the zeolite film was larger than that of the whole membrane under the conditions studied by a factor of 1.3 to 1.7.

Table 4. Pressure drop and concentration polarization at three specific temperatures for CO<sub>2</sub>/CH<sub>4</sub> separation.

T (K)	CO <sub>2</sub> Flux (kg/m <sup>2</sup> h)	ΔP (%)	CPI
299	540	32	0.94
269	453	24	0.94
247	337	17	0.95

To gain further insight on the contribution of adsorption and diffusion selectivities to the observed permselectivity of the membrane, the two terms were determined by modeling. The adsorption selectivity on the feed side was calculated after removing the effect of concentration polarization by calculating adsorbed amounts with the Ideal adsorbed solution theory (IAST) using the adsorption data for adsorption of carbon dioxide and methane in high silica MFI reported by Ohlin et al. [48] and Krishna [49] as input. Since the permselectivity,  $\alpha_{\text{perm}}$ , is known, it is possible to estimate the diffusional selectivity,  $\alpha_{\text{diff}}$ , once the adsorption selectivity has been determined via [50]:

$$\alpha_{\text{perm}} = \alpha_{\text{ads}} \times \alpha_{\text{diff}} \quad (4)$$

The obtained selectivities are presented in Table 5. Both the permselectivity and adsorption selectivities increase with decreasing temperature, whereas the diffusional selectivity shows the opposite trend. The increase in adsorption selectivity with decreasing temperature is expected as carbon dioxide adsorbs stronger and the magnitude of the heat of adsorption is also larger than that for adsorption of methane in zeolite MFI [48]. The reason behind the decrease in diffusion selectivity with decreasing temperature and increasing adsorbed CO<sub>2</sub> load is likely because of the significance of transport via flow-through defects is larger at lower temperatures. Further, since transport through the defects occurs via Knudsen diffusion, which is methane selective, the diffusion selectivity decreases. At the same time, the rate of transport via the zeolite pores decreases with temperature because of both the slower activated diffusion at lower temperature and the increased difficulty in making successful jumps from site-to-site at high adsorbed loadings which slows down the diffusion. In summary, the permselectivity is showing the same trend as the adsorption selectivity when the temperature is altered, it may be concluded that the selectivity is mainly the effect of the adsorption selectivity of the zeolite.

Table 5. Permselectivity for the zeolite film, adsorption selectivity according to IAST and the diffusion selectivity at three different temperatures.

T(K)	$\alpha_{\text{perm.film}}$	$\alpha_{\text{ads}}$	$\alpha_{\text{diff}}$
299	6	28	0.20
269	10	47.3	0.13
247	16	137	0.12

The CO<sub>2</sub>/CH<sub>4</sub> separation factor is shown in Figure 12. The highest separation factor obtained in this study was about 10 at the lowest temperature of 245 K. As pointed out above, carbon dioxide adsorbs stronger than methane in MFI and the difference in affinities is increasing with decreasing temperature as a result of the larger heat of adsorption in MFI for carbon dioxide compared to methane [48]. This leads to an increased CO<sub>2</sub>/CH<sub>4</sub> adsorption selectivity with decreasing temperature. The relatively low separation factor is probably a reason why the effect of concentration polarization is not larger.

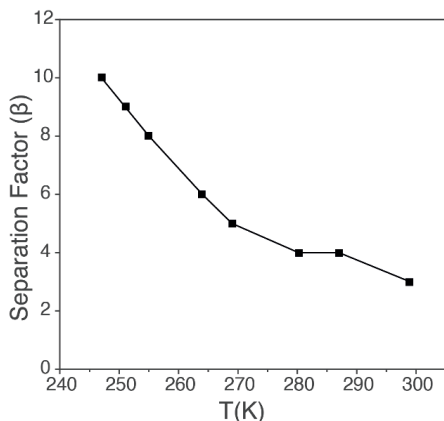


Figure 12. CO<sub>2</sub>/CH<sub>4</sub> separation factor as a function of temperature (Paper I).

### Effect of Si/Al ratio on the separation performance of MFI membranes

As the adsorption selectivity is the dominating contributor to the permselectivity of MFI membranes for the CO<sub>2</sub>/CH<sub>4</sub> separation, it seems natural to investigate how different ways of increasing the adsorption selectivity are affecting the membrane performance. One option for increasing the adsorption selectivity would be to increase the polarity of the zeolite. As carbon dioxide has higher polarizability and is also quadropolar compared to methane which is an octopole [51], the adsorption of carbon dioxide should benefit more from an increased polarity of the framework than the adsorption of methane. Consequently, MFI membranes with three different Si/Al ratios *viz.* 90, 46 and 21 were prepared and evaluated for CO<sub>2</sub>/CH<sub>4</sub> separation. Figures 13-15 show the permeances and separation factors of the three membranes as a function of temperature. It is shown that the CO<sub>2</sub> permeances decreases with decreasing temperature, as expected. Furthermore, the CO<sub>2</sub> permeance decreases with decreasing Si/Al ratio due to the increased transport resistance resulting from the presence of charge balancing cation neutralizing the charge deficit in Al containing zeolites [29] and the longer residence time for CO<sub>2</sub> near Na<sup>+</sup> cation which results in lower overall diffusivity [52].

For the two membranes with the highest Si/Al ratio, the separation factors increased with decreasing temperature down to the lowest investigated temperature, *i.e.* 250 K, while the membrane with the lowest Si/Al ratio displayed a maximum in the separation factor at 271 K. Probably, the adsorption

of CO<sub>2</sub> became too extensive at low temperatures in this, the most polar membrane, resulting in a decrease in the CO<sub>2</sub> transport. The maximum observed separation factors were 2.6 (at 250 K), 7.1 (at 249 K) and 3.3 (at 271 K) for Si/Al ratios of 90, 46 and 21, respectively.

The membrane with highest Si/Al ratio in Paper II and the membrane in Paper I are synthesized with the same synthesis solution, but with different masking techniques and synthesis time. The membrane with the highest Si/Al ratio in Paper II has lower separation factor compared to the membrane in paper I which can be attributed to the greater presence of defects based on their permoporometry patterns. The higher CO<sub>2</sub> permeance of the membrane with highest Si/Al ratio in paper II compared to the membrane in paper I is due to the thinner film (shorter synthesis time) in the former membrane resulting in less well-intergrown film. Consequently, there should be more open grain boundaries in this membrane.

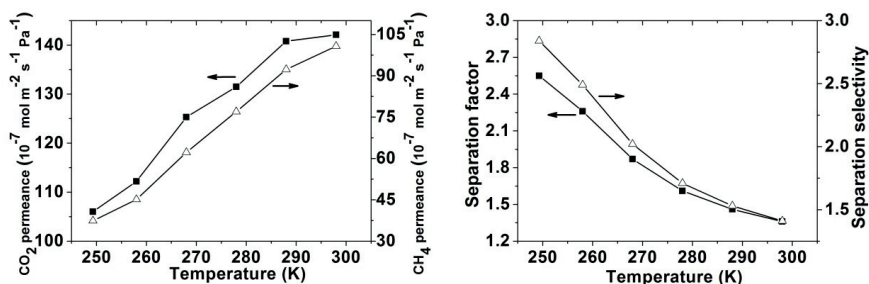


Figure 13. CO<sub>2</sub> and CH<sub>4</sub> permeances(left), separation factor and selectivity(right) for an MFI zeolite membrane with Si/Al =90 for an equimolar CO<sub>2</sub>/CH<sub>4</sub> feed as a function of temperature

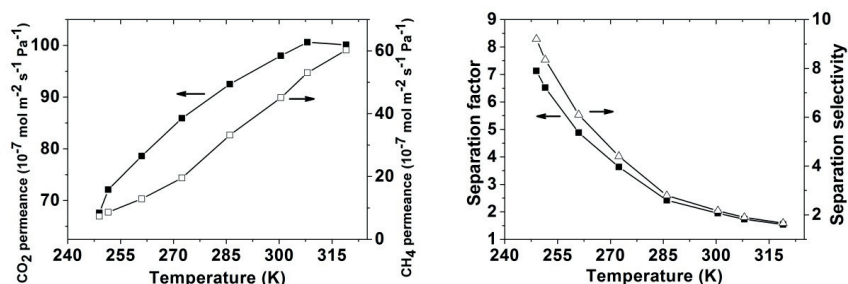


Figure 14. CO<sub>2</sub> and CH<sub>4</sub> permeances(left), separation factor and selectivity(right) for an MFI zeolite membrane with Si/Al =46 for an equimolar CO<sub>2</sub>/CH<sub>4</sub> feed as a function of temperature

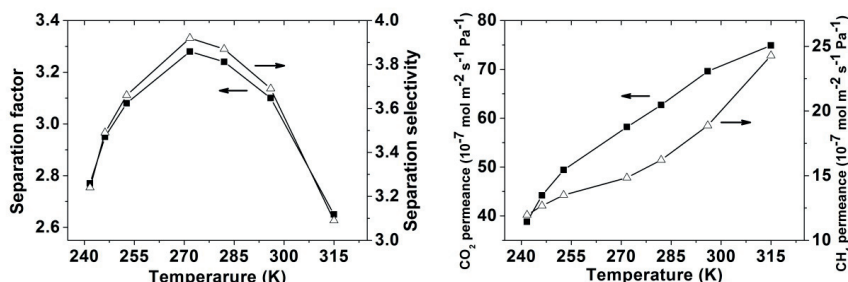


Figure 15. CO<sub>2</sub> and CH<sub>4</sub> permeances(left), separation factor and selectivity(right) for an MFI zeolite membrane with Si/Al =21 for an equimolar CO<sub>2</sub>/CH<sub>4</sub> feed as a function of temperature

## CO<sub>2</sub>/H<sub>2</sub> separation

Synthesized MFI zeolite membranes were evaluated for separation of an equimolar mixture of CO<sub>2</sub> and H<sub>2</sub> which is an important separation in upgrading of synthesis gas. The experiments were performed in a wide temperature range of 235–310 K and at an industrially relevant feed pressure of 9 bar. The separation factor and permeances obtained are presented in Figure 16. The

separation factor is increasing with decreasing temperature whereas the permeance of both components is decreasing. Similarly, as for CO<sub>2</sub>/CH<sub>4</sub> separation, carbon dioxide adsorbs stronger than hydrogen in the zeolite. However, the difference in affinity between carbon dioxide and hydrogen is much greater than for carbon dioxide and methane, and therefore carbon dioxide is essentially filling up the zeolites pores, thus effectively excluding hydrogen from the pore system, resulting in a very CO<sub>2</sub>-selective membrane. The highest CO<sub>2</sub> permeance was about  $78 \times 10^{-7} \text{ mol s}^{-1} \text{ m}^{-2} \text{ Pa}^{-1}$  at around 300 K which is one or two order of magnitude higher than those reported previously in the literature by other research groups [53, 54]. The highest separation factor obtained was 165 at 235 K with a concentration of carbon dioxide in the permeate of 99.4%.

The separation performance of the membrane in terms of both selectivity and flux was superior to that of the previously reported state-of-the-art CO<sub>2</sub>-selective zeolite and polymeric membranes [36, 41].

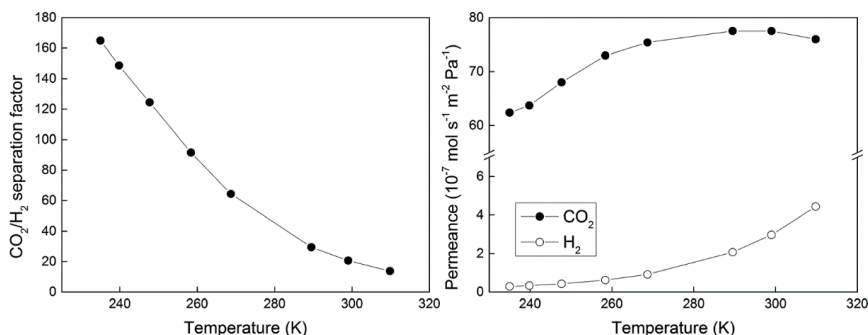


Figure 16. CO<sub>2</sub>/H<sub>2</sub> separation fraction(left), CO<sub>2</sub> and H<sub>2</sub> permeances(right) as a function of temperature for a 50:50 feed at 9 bar total pressure.

## Cost estimation

The economic feasibility of the developed zeolite membranes was assessed by estimating the costs for modules equipped with such membranes prepared as tubes. The costs were also compared to those for the commercially available spiral-wound modules containing MTR Polaris<sup>TM</sup> membranes used in gas processing plant for CO<sub>2</sub>/H<sub>2</sub> separation in commercial-scale [9]. It was assumed that the zeolite membranes were supported on 19-channel  $\alpha$ -alumina tubes having the same permeance as the disc-shaped membranes prepared in our

group. The cost comparison was done for a separation process with a capacity of separating 300 ton CO<sub>2</sub> per day at a CO<sub>2</sub> partial pressure difference across the membrane of 10 bar and room temperature. For such an output, 20 polymeric membrane modules or 1 MFI zeolite membrane module were needed, which indicate much more compact system in case of using zeolite membrane. The module and membrane cost for MFI membrane was approximately 30% lower than the commercial polymeric membrane because of both the high flux MFI membrane resulting in a very low membrane area needed for the separation process and high CO<sub>2</sub>/H<sub>2</sub> selectivity of 26 at 300 K which competes with the selectivity of polymeric membrane which usually show a CO<sub>2</sub>/H<sub>2</sub> selectivity of 10-12 at room temperature. Therefore, high flux ceramic zeolite membranes show great potential for selective, cost-effective and sustainable removal of CO<sub>2</sub> from synthesis gas.



## Conclusions

In the present work, the performance of highly permeable H-ZSM-5 zeolite membranes were evaluated for CO<sub>2</sub>/CH<sub>4</sub> separation which is of high importance for biogas and natural gas purification processes.

The CO<sub>2</sub> flux in CO<sub>2</sub>/CH<sub>4</sub> binary separation was significantly higher than that previously reported in the open literature. The high carbon dioxide permeance was ascribed to the low film thickness, high feed pressure and open and graded support.

Regarding the selectivity, carbon dioxide adsorbs stronger than CH<sub>4</sub> in MFI resulting in a carbon dioxide selective membrane with the selectivity increasing with decreasing temperature. Modeling suggested that pressure drop over the support had a negative effect on the performance of the membrane, whereas the effect of concentration polarization was small. According to the modeling, the membrane selectivity would increase 1.3 to 1.7 times with removing the adverse influence of pressure drop over the support. Decreasing the thickness and increasing the pore size of the top layer of the support would be a means to reduce the support resistance.

The CO<sub>2</sub>/CH<sub>4</sub> diffusion selectivity decreases with decreasing the temperature, unlike the adsorption selectivity. It is likely because the transport in the pores decreases due to both slower diffusion at lower temperatures which also increases the significance of transport via flow-through defects at lower

temperatures and transport via the flow-through defects is CH<sub>4</sub> selective. Therefore, the diffusion selectivity decreases with decreasing temperature. .

The effect of Si/Al ratio on the MFI zeolite membrane performance was studied for the CO<sub>2</sub>/CH<sub>4</sub> separation. MFI membranes with different Si/Al ratio behave differently as the temperature is decreased although they all show an increasing selectivity as the temperature is decreased in the beginning. For the membrane with the lowest Si/Al ratio (or highest Al content), the separation factor reached a maximum followed by a decreasing trend, probably due to very high adsorbed loadings leading to low diffusivity and low driving force. The CO<sub>2</sub> permeance decreased with decreasing Si/Al ratio because of the sodium cations narrowing down the effective pore diameter available for transport and the high affinity of CO<sub>2</sub> to the sodium cations which means that they reside for longer time at these sites, slowing down the transport in the pores.

The economic viability of the developed MFI membranes was estimated and compared to that of the commercially available polymeric membranes in spiral-wound modules. The estimation showed that the cost for the zeolite membranes in a module, was approximately 30% lower than the cost for modules with polymeric membranes.

## **Future work**

This work showed the potential of the highly permeable MFI membranes in CO<sub>2</sub>/CH<sub>4</sub> gas separation. There are several subjects needed to be studied to pursue this work.

Finding the optimal operating pressure and temperature for the membranes to show their best performance for this separation.

The effect of introducing other counter-ions (than sodium) to this type of separation system should be explored.

It would also be very interesting to evaluate ultrathin all-silica chabazite membranes for separating CO<sub>2</sub>/CH<sub>4</sub>. In this framework, the CO<sub>2</sub>/CH<sub>4</sub> selectivity is inherently high due to a molecular sieving mechanism and with an ultra-thin zeolite film, the CO<sub>2</sub> permeance should be high.

It would also be interesting to prepare the membranes as tubes and evaluate their performance at industrially relevant conditions.



## References

1. Abraham, E.R., S. Ramachandran, and V. Ramalingam, *Biogas: Can it be an important source of energy?* Environmental Science and Pollution Research, 2007. **14**(1): p. 67-71.
2. Bauer, A., et al., *Biogas upgrading-Review of commercial technologies*. 2013, SGC Rapport.
3. Petersson, A. and A. Wellinger, *Biogas upgrading technologies—developments and innovations*. 2009: IEA Bioenergy.
4. 2014 6 Oct. 2016; Available from: <http://epp.eurostat.ec.europa.eu/>.
5. Weiland, P., *Biogas production: current state and perspectives*. Applied Microbiology and Biotechnology, 2010. **85**(4): p. 849-860.
6. Ryckebosch, E., M. Drouillon, and H. Veruaeren, *Techniques for transformation of biogas to biomethane*. Biomass & Bioenergy, 2011. **35**(5): p. 1633-1645.
7. Scholz, M., T. Melin, and M. Wessling, *Transforming biogas into biomethane using membrane technology*. Renewable & Sustainable Energy Reviews, 2013. **17**: p. 199-212.
8. *General Information Wobbe Index and Calorimeters*. 6 Oct. 2016; Available from: [http://www.hobre.com/files/products/Wobbe\\_Index\\_general\\_information.pdf](http://www.hobre.com/files/products/Wobbe_Index_general_information.pdf).
9. Baker, R.W. and K. Lokhandwala, *Natural gas processing with membranes: An overview*. Industrial & Engineering Chemistry Research, 2008. **47**(7): p. 2109-2121.
10. Makaruk, A., M. Miltner, and M. Harasek, *Membrane biogas upgrading processes for the production of natural gas substitute*. Separation and Purification Technology, 2010. **74**(1): p. 83-92.
11. *Membranes for clean and renewable power applications*. Woodhead publishing series in energy. 2014, Philadelphia, PA: Woodhead Pub. pages cm.
12. Niesner, J., D. Jecha, and P. Stehlik, *Biogas Upgrading Technologies: State of Art Review in European Region*. 16th International Conference on Process Integration, Modelling and Optimisation for Energy Saving and Pollution Reduction (Pres'13), 2013. **35**: p. 517-522.
13. Tabe-Mohammadi, A., *A review of the applications of membrane separation technology in natural gas treatment*. Separation Science and Technology, 1999. **34**(10): p. 2095-2111.
14. Ebner, A.D. and J.A. Ritter, *State-of-the-art Adsorption and Membrane Separation Processes for Carbon Dioxide Production from Carbon Dioxide Emitting Industries*. Separation Science and Technology, 2009. **44**(6): p. 1273-1421.

15. Giles, D.E., S. Som, and S.K. Aggarwal, *NO<sub>x</sub> emission characteristics of counterflow syngas diffusion flames with airstream dilution*. *Fuel*, 2006. **85**(12-13): p. 1729-1742.
16. Gaetano Iaquaniello, E.A., Barbara Cucchiella, Emma Palo, Annarita Salladini, Alessandra Guarinoni, Andrea Lainati and Luca Basini, *Natural gas catalytic partial oxidation: A way to syngas and bulk chemicals production*. 2012, INTECH Open Access Publisher.
17. Faramawy, S., T. Zaki, and A.-E. Sakr, *Natural gas origin, composition, and processing: A review*. *Journal of Natural Gas Science and Engineering*, 2016. **34**: p. 35-54.
18. Wang, Z., et al., *Syngas composition study*. *Frontiers of Energy and Power Engineering in China*, 2009. **3**(3): p. 369–372.
19. Baker, R.W., *Membrane Technology and Applications*. 2012: John Wiley & Sons.
20. Scott, K. and R. Hughes, *Industrial Membrane Separation Technology*. 2012: Springer Science & Business Media.
21. Sandström, L., *High flux zeolite membranes for efficient production of biofuels*. 2012, Luleå tekniska universitet.
22. Mohanty, K. and M.K. Purkait, *Membrane Technologies and Applications*. 2011: CRC Press.
23. Korelskiy, D., et al., *Efficient ceramic zeolite membranes for CO<sub>2</sub>/H<sub>2</sub> separation*. *Journal of Materials Chemistry A*, 2015. **3**(23): p. 12500-12506.
24. [6 Oct. 2016]; Available from: <http://www.iza-structure.org/databases/>.
25. Jacobs, P.A., et al., *Introduction to zeolite science and practice*. 2001: Elsevier.
26. Turaga, S.C. and S.M. Auerbach, *Calculating free energies for diffusion in tight-fitting zeolite-guest systems: Local normal-mode Monte Carlo*. *Journal of Chemical Physics*, 2003. **118**(14): p. 6512-6517.
27. Noack, M., et al., *Effect of crystal intergrowth supporting substances (ISS) on the permeation properties of MFI membranes with enhanced Al-content*. *Microporous and Mesoporous Materials*, 2006. **97**(1-3): p. 88-96.
28. Comyns, A.E., *Molecular Sieves: Principles of Synthesis and Identification*. R. Szostak. Blackie Academic and Professional, London, 1998. xiv+ 359 pages. ? 79. ISBN 0-7514-0480-2. *Applied Organometallic Chemistry*, 1999. **13**(3): p. 209-210.
29. Noack, M., et al., *Influence of the Si/Al-ratio on the permeation properties of MFI-membranes*. *Microporous and Mesoporous Materials*, 2005. **79**(1-3): p. 329-337.
30. Lai, R. and G.R. Gavalas, *Surface seeding in ZSM-5 membrane preparation*. *Industrial & Engineering Chemistry Research*, 1998. **37**(11): p. 4275-4283.
31. Hunger, M., et al., *Investigation of Internal Silanol Groups as Structural Defects in Zsm-5-Type Zeolites*. *Journal of the Chemical Society-Faraday Transactions I*, 1987. **83**: p. 3459-&.

32. Korelskiy, D., *Quality and performance of zeolite membranes*. 2012, Luleå tekniska universitet.
33. Hedlund, J., et al., *High-flux MFI membranes*. Microporous and Mesoporous Materials, 2002. **52**(3): p. 179-189.
34. Korelskiy, D., et al., *Characterization of flow-through micropores in MFI membranes by permoporometry*. Journal of Membrane Science, 2012. **417**: p. 183-192.
35. Hedlund, J., et al., *Permoporometry analysis of zeolite membranes*. Journal of Membrane Science, 2009. **345**(1-2): p. 276-287.
36. Sandstrom, L., E. Sjoberg, and J. Hedlund, *Very high flux MFI membrane for CO<sub>2</sub> separation*. Journal of Membrane Science, 2011. **380**(1-2): p. 232-240.
37. Kosinov, N., et al., *High flux high-silica SSZ-13 membrane for CO<sub>2</sub> separation*. Journal of Materials Chemistry A, 2014. **2**(32): p. 13083-13092.
38. Tian, Y.Y., et al., *Synthesis of a SAPO-34 membrane on macroporous supports for high permeance separation of a CO<sub>2</sub>/CH<sub>4</sub> mixture*. Journal of Materials Chemistry, 2009. **19**(41): p. 7698-7703.
39. van den Bergh, J., et al., *Natural gas purification with a DDR zeolite membrane; permeation modelling with maxwell-stefan equations*. From Zeolites to Porous Mof Materials: The 40th Anniversary of International Zeolite Conference, Proceedings of the 15th International Zeolite Conference, 2007. **170**: p. 1021-1027.
40. S., Y., et al., *DDR-type zeolite membrane synthesis, modification and gas permeation studies*. Journal of Membrane Science, 2016. **505**: p. 194-204.
41. Baker, R.W. and B.T. Low, *Gas Separation Membrane Materials: A Perspective*. Macromolecules, 2014. **47**(20): p. 6999-7013.
42. Mintova, S., et al., *Variation of the Si/Al ratio in nanosized zeolite Beta crystals*. Microporous and Mesoporous Materials, 2006. **90**(1-3): p. 237-245.
43. Krishna, R. and J.M. van Baten, *Kinetic Monte Carlo Simulations of the loading dependence of diffusion in zeolites*. Chemical Engineering & Technology, 2005. **28**(2): p. 160-167.
44. Krishna, R. and J.M. van Baten, *Maxwell-Stefan modeling of slowing-down effects in mixed gas permeation across porous membranes*. Journal of Membrane Science, 2011. **383**(1-2): p. 289-300.
45. Yu, L., et al., *Very high flux MFI membranes for alcohol recovery via pervaporation at high temperature and pressure*. Separation and Purification Technology, 2015. **153**: p. 138-145.
46. Korelskiy, D., et al., *High flux MFI membranes for pervaporation*. Journal of Membrane Science, 2013. **427**: p. 381-389.
47. Ye, P.C., et al., *Efficient Separation of N<sub>2</sub> and He at Low Temperature Using MFI Membranes*. Aiche Journal, 2016. **62**(8): p. 2833-2842.

48. Ohlin, L., et al., *Adsorption of CO<sub>2</sub>, CH<sub>4</sub>, and H<sub>2</sub>O in Zeolite ZSM-5 Studied Using In Situ ATR-FTIR Spectroscopy*. Journal of Physical Chemistry C, 2013. **117**(33): p. 16972-16982.
49. Krishna, R., *The Maxwell-Stefan description of mixture diffusion in nanoporous crystalline materials*. Microporous and Mesoporous Materials, 2014. **185**: p. 30-50.
50. van de Graaf, J.M., F. Kapteijn, and J.A. Moulijn, *Modeling permeation of binary mixtures through zeolite membranes*. Aiche Journal, 1999. **45**(3): p. 497-511.
51. Lide, D.R., *CRC handbook of chemistry and physics*. 84 ed. 2003-2004: CRC Press.
52. Newsome, D. and M.O. Coppens, *Molecular dynamics as a tool to study heterogeneity in zeolites - Effect of Na<sup>+</sup> cations on diffusion of CO<sub>2</sub> and N<sub>2</sub> in Na-ZSM-5*. Chemical Engineering Science, 2015. **121**: p. 300-312.
53. Hong, M., et al., *Hydrogen purification using a SAPO-34 membrane*. Journal of Membrane Science, 2008. **307**(2): p. 277-283.
54. Kusakabe, K., et al., *Gas permeation properties of ion-exchanged faujasite-type zeolite membranes*. Aiche Journal, 1999. **45**(6): p. 1220-1226.





# PAPER I

---

**CO<sub>2</sub>/CH<sub>4</sub> separation by highly permeable H-ZSM-5 membranes**

Shahpar Fouladvand, Danil Korelskiy, Liang Yu, Jonas Hedlund and Mattias Grahn.

*To be submitted*



# CO<sub>2</sub>/CH<sub>4</sub> separation by highly permeable H-ZSM-5 membranes

Shahpar Fouladvand\*, Danil Korelskiy, Liang Yu, Jonas Hedlund and Mattias Grahn

Chemical Technology, Luleå University of Technology, SE-971 87 Luleå, Sweden

\* Corresponding author. E-mail: shahpar.fouladvand@ltu.se, tel.: +46-920-49-1419

## Abstract

Ultra-thin H-ZSM-5 zeolite membranes were prepared on porous graded  $\alpha$ -alumina supports. Two membranes with varying quality was evaluated for separation of a 50:50 (v:v) mixture of CO<sub>2</sub> and CH<sub>4</sub> in a temperature range of *ca.* 250–300 K and at a feed pressure of 9 barA and a permeate pressure of 1 barA. No sweep gas as used. The membranes were found to be CO<sub>2</sub>-selective in the entire temperature range. The selectivity toward CO<sub>2</sub> was increasing with decreasing temperature, most likely due to the stronger CO<sub>2</sub> adsorption at lower temperatures. At the lowest temperature studied of *ca.* 250 K, the high quality membrane displayed a CO<sub>2</sub>/CH<sub>4</sub> separation factor of 10 with a CO<sub>2</sub> flux as high as 337 kg m<sup>-2</sup> h<sup>-1</sup>. The CO<sub>2</sub> permeance observed in the present work was superior to values previously reported in the open literature. Modeling showed that pressure drop over the support had an adverse effect on the membrane performance whereas concentration polarization was negligible. Furthermore, it was shown experimentally that defects in the low quality membrane reduced the separation performance.

**Keywords:** Biogas upgrading, H-ZSM-5 zeolite, membrane, CO<sub>2</sub>/CH<sub>4</sub> separation, modeling

## 1. Introduction

Seeking of sustainable energy sources has recently become one of the major topics on the energy agenda due to the fact that the oil reserves are finite and

will eventually run out. In addition, there has been a growing concern over the rapidly increasing concentration of carbon dioxide in the atmosphere, as being one of the causes for climate change [1]. Biogas, produced via anaerobic digestion of biomass is a renewable source of energy with great potential as a substitute for natural gas, considering the vast amounts of organic waste produced every day. However, the biogas has to be upgraded before utilization in many applications, which involves separation of carbon dioxide from the gas, since it lowers the heating value and may also cause corrosion of pipes and fittings [2].

Separation of CO<sub>2</sub> from natural gas is the largest gas separation process and of tremendous importance to society. The total worldwide natural gas production is about 122 trillion cubic feet per year in 2014 and it is growing [3]. The CO<sub>2</sub> content in natural gas varies considerably depending on the source of the gas [4] and based on the US pipeline specification, the CO<sub>2</sub> content must be reduced to be < 2%. Separation by absorption in amine solutions is the most common method for CO<sub>2</sub> removal from natural gas [4]. The membrane market share in natural gas upgrading is less than 5% [4], but is expected to increase because of rapid development in the membrane area. The technologies used for upgrading natural gas have been transferred also to upgrading of biogas [5]. Today, water scrubbing, pressure swing adsorption (PSA), chemical scrubbing are the most widely technologies used for biogas upgrading [6].

Over the recent years, membrane separation processes have received a lot of attention because of their simplicity, low energy demands and high efficiency and are considered to be one of the most promising alternatives to the current CO<sub>2</sub> separation technologies [2, 7]. The current commercial-scale membrane technology for CO<sub>2</sub> separation is based on polymer membranes. These polymer membrane materials are quite inexpensive and relatively easy to prepare. However, the steel modules used for housing of the membranes are very expensive and these membranes are prone to plasticization at high partial pressures of carbon dioxide leading to a reduced performance of the membranes. Additionally, polymer membranes have limited thermal stability. The commercial cellulose acetate membranes which are most widely used for natural gas sweetening typically have CO<sub>2</sub>/CH<sub>4</sub> separation selectivity of 10-20 and CO<sub>2</sub> permeance of 60-110 GPU [4, 8]. These commercial membranes require large

membrane areas and many steel modules for the separation process because of their relatively low CO<sub>2</sub> permeance. Compared to polymer membranes, zeolite membranes show better thermal and chemical stability and often also much higher permeances because of their microporous structure. Zeolite membranes have also shown significantly higher selectivities than polymeric membranes [9]. In addition, ultra-thin zeolite membranes have recently been shown to be economically viable and more cost-effective for CO<sub>2</sub>/H<sub>2</sub> separation than commercial polymer membranes due to much higher permeance *viz.* a factor of almost 10 times higher than commercial polymer membranes [7]. Most investigations on the use of zeolite membranes for separating carbon dioxide from methane have focused on small pore zeolites, such as CHA and DDR. In such zeolites the pore openings are small enough (3.8 Å or smaller) to significantly slow down the diffusion of the bulkier methane molecule, whereas the more slender carbon dioxide can still diffuse through the pores resulting in high CO<sub>2</sub>/CH<sub>4</sub> selectivities [10]. Although high selectivity has been demonstrated by these small pore zeolites, so far membranes with rather low permeance have been reported [11]. This is probably due to the fact that the zeolite membranes described showed film thicknesses exceeding 1 µm. Kosinov et al reported a CO<sub>2</sub>/CH<sub>4</sub> selectivity of 42 with a CO<sub>2</sub> permeance of  $3 \times 10^{-7}$  mol m<sup>-2</sup> s<sup>-1</sup> Pa<sup>-1</sup> for CHA (SSZ-13) membrane at a feed pressure of 6 bar and a temperature of 293 K [11]. Tian et al. reported room temperature separation selectivity of 9 and a CO<sub>2</sub> permeance of  $25 \times 10^{-7}$  mol m<sup>-2</sup> s<sup>-1</sup> Pa<sup>-1</sup> for a SAPO-34 (CHA) membrane [12]. Van den Bergh et al. also reported a CO<sub>2</sub>/CH<sub>4</sub> selectivity exceeding 3000 at 225 K for a DDR membrane. However, the small pores in DDR probably also contribute to the resulting low CO<sub>2</sub> permeance observed of about  $1.0 \times 10^{-7}$  mol m<sup>-2</sup> s<sup>-1</sup> Pa<sup>-1</sup> [13]. Recently, Yang et al. reported a CO<sub>2</sub>/CH<sub>4</sub> selectivity of a DDR membrane of 92 for a feed mixture of 90% CO<sub>2</sub>-10% CH<sub>4</sub> and a low CO<sub>2</sub> permeance of  $1.8 \times 10^{-7}$  mol m<sup>-2</sup> s<sup>-1</sup> Pa<sup>-1</sup> at a pressure of 2 bar and a temperature of 297 K [14].

Separation of CO<sub>2</sub>/CH<sub>4</sub> mixtures by medium pore zeolite membranes has also been reported. Poshusta et al. found that the separation selectivity decreases with increasing temperature and their highest CO<sub>2</sub>/CH<sub>4</sub> mixture selectivity for H-ZSM-5 membrane was 5.5 at room temperature and the feed pressure of 2.7 bar [15]. We have previously evaluated ultra- thin MFI membranes for CO<sub>2</sub>/CH<sub>4</sub> separation and reported a separation selectivity of 6.2 and a CO<sub>2</sub> permeance of

$45 \times 10^{-7} \text{ mol m}^{-2} \text{ s}^{-1} \text{ Pa}^{-1}$  at feed pressure of 10 bar and a temperature of 277 K [2]. In the present work, the effect of temperature on the  $\text{CO}_2/\text{CH}_4$  separation performance for ultra-thin MFI membranes was evaluated. Furthermore, high and low quality MFI membranes were chosen to study the effect of presence of flow-through defects on the separation performance and gas permeance.

## 2. Experimental

### 2.1. Membrane preparation

H-ZSM-5 zeolite membranes with a zeolite film thickness and a Si/Al ratio of *ca.* 0.5  $\mu\text{m}$  and 139, respectively, [16] were prepared according to the procedure reported in detail previously [17] and briefly here. Graded  $\alpha$ -alumina disks (Fraunhofer IKTS, Germany) were used as supports to provide mechanical strength to the thin zeolite film. The supports were masked with wax (C105, Carbona AB) to prevent zeolite invasion into the support during synthesis. After masking, the zeolite film was prepared by firstly rendering the surface of the support positively charged by depositing a cationic polymer on the surface of the support. Thereafter, the support was immersed in a sol containing 50 nm colloidal MFI crystals to create a monolayer of crystals on the support. The seeded support was then immersed in a synthesis solution with the following molar composition: 3TPAOH: 25SiO<sub>2</sub>: 1450H<sub>2</sub>O: 100C<sub>2</sub>H<sub>5</sub>OH. The synthesis was carried out in a heated oil bath at 361 K for 72 hours. After synthesis, the membranes were thoroughly rinsed with a 0.1 M ammonia solution and then calcined at 773 K for 6 hours with a heating and cooling rate of 0.2 and 0.3 K/min, respectively.

### 2.2. Membrane characterization

Morphology and film thickness of the membranes were characterized by scanning electron microscopy (SEM) using an FEI Magellan 400 field emission XHR-SEM operating at an accelerating voltage of 1 kV. The samples were not coated prior to the analysis.

*n*-Hexane/helium adsorption-branch permoporometry [17] analysis was performed to assess the quality of the membranes by measuring the size distribution of flow-through defects in the zeolite membranes. The method and data evaluation are described in detail in a previous publication [18]. In short,

the membrane was first mounted in a stainless steel Wicke–Kallenbach cell sealed with graphite gaskets and thereafter the membrane was dried at 573 K for 6 h in a helium flow (99.999%, AGA). The pressure difference across the membrane was 1 bar with an atmospheric permeate pressure. The permeance of helium through the membrane was determined as a function of the amount of *n*-hexane in the feed. The relative pressure of *n*-hexane was increased gradually from 0 up to 0.38, and the system was allowed to equilibrate at each measuring point. The width of defects smaller and larger than 2 nm was estimated by the Horvath-Kawazoe (H-K) equation and the Kelvin equation, respectively. The defect area distribution was calculated from the measured helium molar flow and helium molar flux through the defects estimated from Fick's law. Defect distribution was evaluated in terms of relative areas of defects (area of defects divided by the total membrane area).

### 2.3. Single gas permeation experiments

After characterization by permoporometry, the membrane retained in the cell was again dried at 573 K for 6 h at a heating rate of 1 °C/min in a helium flow. Afterwards, single gas CO<sub>2</sub> and CH<sub>4</sub> permeances were measured in the temperature range of 250–300 K. During the single gas experiment, the feed pressure was kept at 4.5 barA whereas atmospheric pressure was used on the permeate side.

### 2.4. Separation experiments

The membrane was kept in the stainless steel cell and dried at 573 K for 6 hours in a helium flow prior to the separation experiments. Mass flow controllers (SLS500, Brooks Instrument) were used to adjust the feed flow rate and composition. The feed was equimolar in CO<sub>2</sub> (99.995%, AGA) and CH<sub>4</sub> (99.9995%, AGA) and the total flow rate was 10 l/min. The pressure on the feed- and permeate side was 9 and 1 barA, respectively, adjusted by a back pressure regulator. A mass spectrometer (GAM400, InProcess Instrument) was used to analyze the composition of the permeate stream. The permeate volumetric flow rate was measured by a drum type gas meter (TG 5, Ritter Apparatebau GmbH). The separation experiment was carried out in the same temperature range as used for the single gas permeation experiments, *i.e.* 250–300 K. The membrane selectivity  $\alpha$  was defined as  $\alpha = \Pi_i/\Pi_j$  which is the component single permeance ratio and the separation factor  $\beta$  was calculated as

follows  $\beta = (y_i/y_j)/(x_i/x_j)$ , where  $y$  and  $x$  is the molar fraction of components  $i$  and  $j$  in the permeate and feed stream, respectively. During the experiment, the temperature in the membrane cell was monitored by a type K thermocouple connected to the feed side of the membrane.

### 3. Modeling

The performance of high flux composite membranes may be affected by concentration polarization on the feed side as well as pressure drop over the support [19-21]. Both of these effects decreases the performance, in terms of flux and selectivity, of the membrane and it is therefore of interest to estimate to which extent the experiments reported in this work were affected by these phenomena. We have previously described the model used for assessing these effects in detail and therefore we only describe the procedure briefly herein [19-21].

Concentration polarization on the feed side may be assessed by determining the concentration polarization index:

$$\frac{n_m}{n_b} = \exp(J_v / k_c) + \frac{n_p}{n_b} [1 - \exp(J_v / k_c)] \quad (1)$$

where  $n_m$  is the mole fraction at the zeolite film - gas interface and  $n_b$  is the mole fraction in the gas bulk,  $k_c$  is the mass transfer coefficient, further  $J_v$  is the volumetric flux and  $n_p$  is the mole fraction in the permeate. The mass transfer coefficient may be obtained from the Sherwood number:

$$Sh = \frac{k_c d_h}{D} \quad (2)$$

where  $d_h$  is the hydraulic diameter of the cell and  $D$  is the gas phase diffusivity of carbon dioxide. The Sherwood number is obtained from correlations relating the Sherwood (Sh) number to the Reynolds (Re) and Schmidt (Sc) numbers. Perdana et al. have reported a correlation for mass transfer in a Wicke-Kallenbach cell [22].

$$\text{Sh} = 2.83 + 2.24 \text{Re}^{0.58} \text{Sc}^{0.33} \left( \frac{w}{D_C} \right)^{1.30} \quad (3)$$

where  $w$  is the compartment height *i.e.* the thickness of the gas film on the feed side of the membrane and  $D_C$  is the diameter of the membrane inside the gaskets, for details see Perdana et al. [22]. In the original work by Perdana et al, the Reynolds numbers were low and the membrane was operating under laminar flow. In this work, the Reynolds number were much higher indicating turbulent flow, consequently we changed the exponent of the Reynolds number in equation (3) to 0.8 to reflect the change in Sherwood number with Reynolds number at turbulent conditions [23].

The pressure drop over each layer of the support was determined using the same methodology as described in detail elsewhere [20, 24-26]. Transport through the 3 mm thick base layer having 3  $\mu\text{m}$  pores was assumed to occur via viscous flow, whereas transport through the 30  $\mu\text{m}$  thick top layer was assumed to occur via a combination of viscous flow and Knudsen diffusion. Effective Knudsen transport coefficients and permeabilities for each layer have been determined for the support used previously [20].

Viscosities and gas phase diffusivities were adjusted to the desired temperature using Sutherland's equation [27] and the  $D_i \propto T^{3/2}$  relationship, respectively. Mixture viscosities were estimated as molar fraction weighted averages. The ideal adsorbed solution theory (IAST) was used for estimating adsorbed concentrations on the feed side of the membrane during separation [28]. Saturation loadings, Langmuir affinity coefficients and adsorption enthalpies were taken from Ohlin et al. and Krishna [29, 30].

Once the contributions from the concentration polarization and pressure drop over the support have been determined, a corrected permselectivity for the zeolite film itself can be calculated as:

$$\alpha_{perm, film} = \frac{J_{\text{CO}_2} / \left( \left( \frac{n_m}{n_b} \right) \times P_{\text{CO}_2, \text{feed}} - P_{\text{CO}_2 \text{ perm, film}} \right)}{J_{\text{CH}_4} / \left( P_{\text{total, feed}} - P_{\text{CO}_2, \text{feed}} \times \left( \frac{n_m}{n_b} \right) - P_{\text{CH}_4 \text{ perm, film}} \right)} \quad (4)$$

where  $J_i$  is the flux of component  $i$  through the membrane and  $P_{i, \text{perm, film}}$  is the partial pressure of component  $i$  at the interface between the support and the zeolite film.

Further, the permselectivity of zeolite membranes may, to a first approximation, be expressed as the product of the diffusion- and adsorption selectivities [31]:

$$\alpha_{\text{Perm, film}} = \alpha_{\text{diff}} \times \alpha_{\text{ads}} = \frac{\Pi_i}{\Pi_j} = \frac{D_i S_i}{D_j S_j} \quad (5)$$

where  $D_i$  and  $D_j$  are the diffusion coefficient of components  $i$  and  $j$ , respectively and  $S_i$  and  $S_j$  are the ratios of the mole fractions in the adsorbed phase and gas phase for component  $i$  and  $j$ , respectively. The composition of the adsorbed phase was determined using the IAST as described above. Once the adsorption selectivity has been determined, the diffusion selectivity may be determined from equation (5).

## 4. Results and discussion

### 4.1. Membrane characterization

Figure 1 shows SEM top view (a, c) and cross section (b) images of membranes M1 and M2. The zeolite films in both membranes have a thickness of *ca.* 450 nm. The zeolite film in membrane M1 (Figure a, b) is even and composed of well-intergrown zeolite crystals, free from large defects (*e.g.* cracks and pinholes) whilst the presence of defects in the forms of cracks can be noticed in membrane M2 (Figure c).

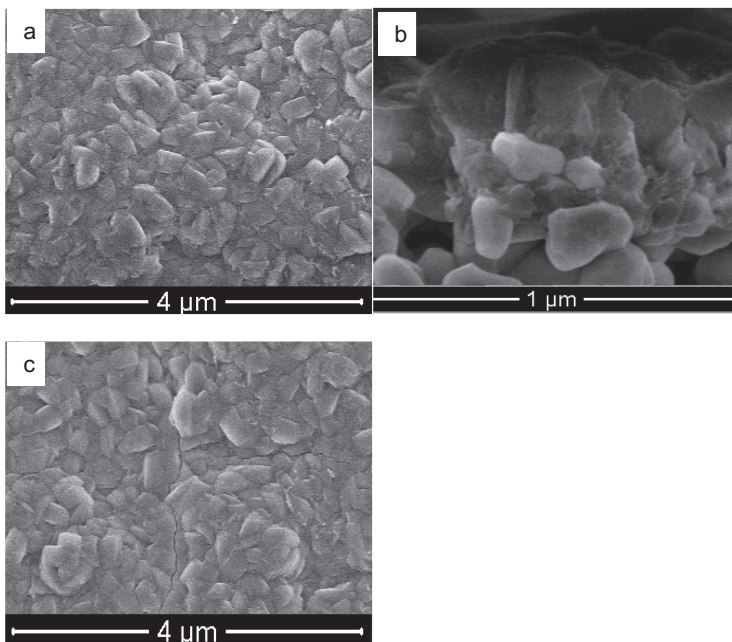


Figure 1. SEM images of the membrane M1: (a) top and (b) cross-section views, membrane M2: (c) top view.

Figure 2 shows *n*-hexane/helium permoporometry patterns for both membranes. The initial helium permeance, measured at the relative pressure of *n*-hexane ( $p/p_0$ ) of 0 was high for both membranes, *viz.*  $41 \times 10^{-7}$  and  $76.33 \times 10^{-7} \text{ mol s}^{-1} \text{ m}^{-2} \text{ Pa}^{-1}$ , for membranes M1 and M2, respectively. At a relative pressure of *n*-hexane of  $3.7 \times 10^{-4}$ , the helium permeance was reduced to  $0.058 \times 10^{-7}$  and  $12.66 \times 10^{-7} \text{ mol s}^{-1} \text{ m}^{-2} \text{ Pa}^{-1}$ , *i.e.* by about 99.8% and 83% for membrane M1 and M2, respectively. At this relative pressure, the zeolite pores and micropore defects with a width smaller than 0.73 nm should be blocked. This indicates that the majority of the pores in the membrane M1 should be small micropores mainly in the form of open grain boundaries. By further increasing the *n*-hexane concentration in the feed, the He permeance of membrane M1 was gradually reduced to as low as  $0.033 \times 10^{-7} \text{ mol s}^{-1} \text{ m}^{-2} \text{ Pa}^{-1}$  at the final relative pressure of 0.34. For membrane M1, about 77.2% of the defects were micropores smaller than 2 nm. For membrane M2, the final He permeance was reduced to  $0.13 \times 10^{-7} \text{ mol s}^{-1} \text{ m}^{-2} \text{ Pa}^{-1}$  at the relative pressure of 0.38, indicating the presence of defects mainly in the range of 0.71- 1.78 nm. The defect distribution in terms of relative areas for membrane M1 and M2 is presented in Table 1 and 2 for comparison.

The total relative area of defects was estimated to be as small as 0.001% of the total membrane area for membrane M1 and 1.1% for membrane M2.

Table 1. Permporometry data for membrane M1.

P/P0	Permeance ( $10^{-7} \text{ mol s}^{-1} \text{ m}^{-2} \text{ Pa}^{-1}$ )	Defect interval (nm)	Relative area of defects <sup>a</sup> (%)
0	41		
0.00026	0.059		
0.00037	0.058	0.71 - 0.73	0.000034
0.0011	0.056	0.73 - 0.80	0.00024
0.012	0.056	0.80 - 1.04	0.0000
0.11	0.033	1.04 - 1.78	0.00058
0.34	0.033	1.78 - 4.20	0.00000
		> 4.20	0.00024
		Total	0.0011

<sup>a</sup> Area of defects per total membrane area

Table 2. Permporometry data for membrane M2.

P/P0	Permeance ( $10^{-7} \text{ mol s}^{-1} \text{ m}^{-2} \text{ Pa}^{-1}$ )	Defect interval (nm)	Relative area of defects <sup>a</sup> (%)
0	76.33		
0.00022	16.08		
0.00037	12.66	0.71 - 0.73	0.36
0.00111	7.11	0.73 - 0.80	0.47
0.011	1.88	0.80 - 1.04	0.27
0.12	0.49	1.04 - 1.78	0.034
0.38	0.13	1.78 - 4.52	0.004
		> 4.52	0.0009
		Total	1.14

<sup>a</sup> Area of defects per total membrane area

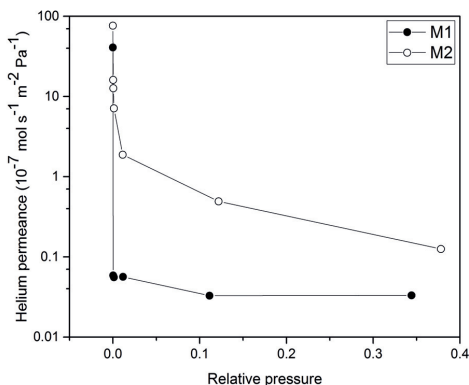


Figure 2. Permporometry patterns determined for membranes M1 and M2.

#### 4.2. Single gas permeation data

Figure 3 shows single gas permeances of CO<sub>2</sub> and CH<sub>4</sub> measured as a function of temperature for membrane M1 at 4.5 barA feed pressure *i.e.* the same pressure as the feed partial pressures in the separation experiments. The single gas permeance of CH<sub>4</sub> was almost constant (varied less than 10%) and higher than that of CO<sub>2</sub> in the entire temperature range. The permeance of CO<sub>2</sub> on the contrary was much lower and decreased with decreasing temperature in the entire temperature range. To understand these trends, we calculated the driving force, expressed as difference in adsorbed loading, over the zeolite film after adjusting the pressure on the permeate side for pressure drop over the support. We used the adsorption data previously reported by Ohlin et al. for adsorption of CO<sub>2</sub> and CH<sub>4</sub> in high silica MFI [30]. For CO<sub>2</sub>, the driving force decreased from 0.31 to 0.095 mol g<sup>-1</sup> when the temperature was decreased from 290K to 250K. The reason for this was that the adsorbed loading on the permeate side of the membrane increased faster than the adsorbed loading on the feed side of the membrane as the temperature was decreased, resulting in a smaller driving force over the film at lower temperatures. For CH<sub>4</sub> on the other hand, the driving force was rather constant (varied less than 10%), *i.e.* *ca.* 0.36 mol g<sup>-1</sup> at 250 and 290 K *ca.* 0.39 mol g<sup>-1</sup> at 265 K. It should be noted that, the driving forces for CH<sub>4</sub> is larger than those for CO<sub>2</sub> as is the diffusivity of CH<sub>4</sub> in zeolite MFI [32]. The higher diffusivity and driving force therefore explains the higher observed permeance of CH<sub>4</sub> as compared to CO<sub>2</sub>.

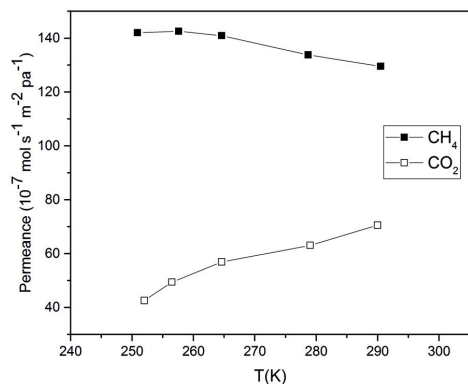


Figure 3. Single gas permeances as a function of temperature for membrane M1 at 4.5 bar feed pressure.

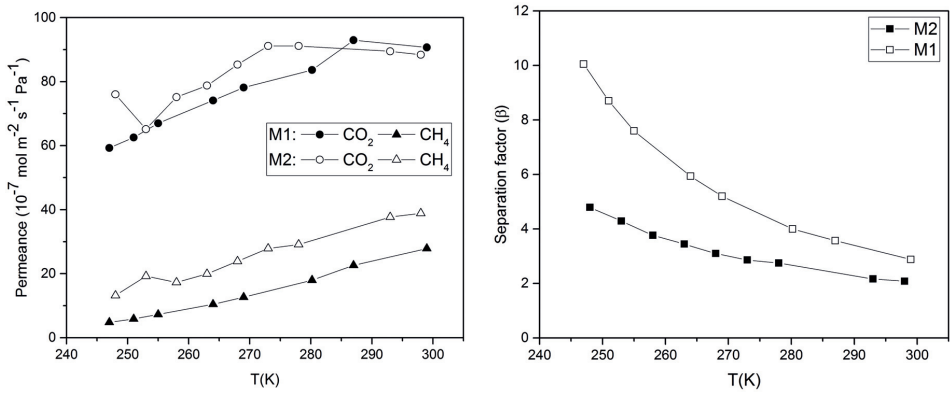
#### 4.3. CO<sub>2</sub>/CH<sub>4</sub> separation

Table 3 shows the obtained CO<sub>2</sub>/CH<sub>4</sub> separation data, including CO<sub>2</sub> and CH<sub>4</sub> fluxes and selectivities of the membranes at different temperatures. The high quality membrane, M1, showed a very high mixture CO<sub>2</sub> permeance varying from  $90 \times 10^{-7} \text{ mol s}^{-1} \text{ m}^{-2} \text{ Pa}^{-1}$  at the highest temperature to about  $60 \times 10^{-7} \text{ mol s}^{-1} \text{ m}^{-2} \text{ Pa}^{-1}$  at the lowest temperature, see Figure 4. The mixture CO<sub>2</sub> permeances are quite similar as the single gas CO<sub>2</sub> permeances. The CO<sub>2</sub> permeance of about  $90 \times 10^{-7} \text{ mol s}^{-1} \text{ m}^{-2} \text{ Pa}^{-1}$  is, to the best of our knowledge, the highest value reported in the open literature. The mixture CH<sub>4</sub> permeance was lower than the single gas CH<sub>4</sub> permeance, showing that CO<sub>2</sub> is partially blocking the transport of CH<sub>4</sub> in the mixture separation experiment. Similar findings have been reported by other groups [33-35].

The separation factor (Figure 4) and selectivities varied in the range 3-10 and 3-12, respectively, for the high quality membrane with the highest separation factor and selectivity observed at the lowest temperature.

Table 3. Flux and selectivities for the membranes.

T (K)	CO <sub>2</sub> flux (kg m <sup>-2</sup> h <sup>-1</sup> )		CH <sub>4</sub> flux (kg m <sup>-2</sup> h <sup>-1</sup> )		Selectivity ( $\alpha$ )	
	M1	M2	M1	M2	M1	M2
248	337	433	12.2	32.9	12	6
252	357	419	15.0	48.5	11	3
258	384	442	18.4	43	9	4
263	428	465	26.3	49.2	7	4
268	453	497	31.8	58.4	6	4
278	490	534	44.7	71	5	3
298	540	536	68.4	94	3	2

Figure 4. Permeances through membranes M1 and for an equimolar feed mixture as a function of temperature (left), CO<sub>2</sub>/CH<sub>4</sub> Separation factor as a function of temperature (right).

We have previously shown that both permeances and selectivities for our membranes are adversely affected by pressure drop over the support and concentration polarization on the feed side in high flux separations [19-21]. In the present work, the pressure drop over the support was evaluated at three different temperatures to capture the trend over the investigated temperature range. The relative pressure drop of carbon dioxide over the support varies from ca 32% at the highest temperature where the flux also is highest, to ca 17 % at 247 K where the flux is lowest, see Table 4, showing that the support is decreasing the performance of the membrane in concert with previous findings. Most of the resistance in the support is in the top layer having small, ca 100 nm, pores. Thus, either increasing the pore size or reducing the thickness of the top layer would reduce the influence of the support. Reducing the thickness of the top layer from 30  $\mu$ m to 5-10  $\mu$ m would improve the situation significantly [36].

The influence of concentration polarization on the membrane performance was also assessed by determining the concentration polarization index at the same three temperatures using equation 1, see Table 4.

Table 4. Relative pressure drop over the support ( $\Delta P$ ), concentration polarisation index (CPI), selectivity for the zeolite film ( $\alpha_{\text{perm, film}}$ ) and adsorption selectivity ( $\alpha_{\text{ads}}$ ) according to IAST estimated at three different temperatures for membrane M1 and Diffusion selectivity ( $\alpha_{\text{ads}}$ ) of membrane M1 and M2.

T (K)	$\Delta P$ (%)	CPI	$\alpha_{\text{perm, film}}$	$\alpha_{\text{ads}}$	$\alpha$ diff (membrane M1)	$\alpha$ diff (membrane M2)
299	32	0.94	6	28	0.20	0.12
269	24	0.94	10	47.3	0.13	0.07
247	17	0.95	16	137	0.12	0.06

For membrane M1, the concentration polarization index was about 0.94 at all temperatures studied, which indicates that concentration polarization was small or negligible at these experiments despite the high flux, as a result of the relatively low selectivity of the membrane.

The  $\text{CO}_2/\text{CH}_4$  selectivity was increasing with decreasing temperature. The highest selectivity of 12 was observed at the lowest temperature studied of 247 K for membrane M1, see Table 3. Figure 4 shows the  $\text{CO}_2/\text{CH}_4$  separation factor as a function of temperature. For membrane M1, the lowest separation factor of 3 was observed at the highest temperature investigated of 300 K. With decreasing temperature, the separation factor increased, reaching nearly 10 at 247 K. Poshusta et al. have also reported increasing separation selectivity with decreasing temperature for  $\text{CO}_2/\text{CH}_4$  separation through MFI zeolite membrane [15]. The same trend with a lower separation factor range which is the result of the presence of defects is also observed for membrane M2. Carbon dioxide adsorbs stronger than methane in zeolite MFI and as the heat of adsorption for carbon dioxide also is larger (more negative) than that of methane, the  $\text{CO}_2/\text{CH}_4$  adsorption selectivity is increasing with decreasing temperature [37]. Table 4 shows the  $\text{CO}_2/\text{CH}_4$  adsorption selectivities on the feed side determined at three

different temperatures using the Ideal adsorbed solution theory. Adsorption data for carbon dioxide and methane in high silica MFI reported by Ohlin et al. and Krishna was used as input [29, 30]. The calculations were performed after removing the effect of concentration polarization. The estimated adsorption selectivity increases with decreasing temperature, from ca 28 at 300K to ca 137 at 247K. Consequently, the zeolite is adsorption selective towards carbon dioxide and the selectivity is increasing with decreasing temperature, in concert with previous findings [2, 15]. With the pressure drop over the support and concentration polarization index determined, it is now possible to determine corrected permselectivities for the zeolite film alone. These corrected permselectivities are a factor of 1.3 to 1.7 larger than the measured ones, ranging from ca 6 to 16, see Table 4.

as the permselectivities and adsorption selectivities now have been determined we can now also determine the diffusion selectivity from equation 4. The diffusion selectivities for both membranes are presented in table 4. For both membranes the diffusion selectivities decreases by about a factor 2 with decreasing temperature in the investigated temperature range 299K to 247K. The diffusion selectivities for membrane M2 is also significantly lower than the corresponding for membrane M1, this is most likely due to larger amounts of defects in the former membrane as shown by permoporometry.

At the experimental conditions prevailing here, the adsorbed loading of carbon dioxide is rather high and it is well known that correlation effects (diffusional coupling) are typically significant in the MFI framework at high loadings. Indeed, MD simulation performed for similar conditions as in this work, suggest that correlation effects are strong at these conditions. However, correlation effects do not explain the decrease in diffusion selectivity with decreasing temperature (and increasing adsorbed loading). Instead we propose that transport via flow-through defects is becoming increasingly important as the temperature is decreased. As the transport through the defects occurs via Knudsen diffusion, which is methane selective, this may probably explain the decreased diffusion selectivity with decreasing temperature. Furthermore, the more defective membrane M2 displayed lower diffusion selectivities, which shows that defects reduce diffusion selectivity as discussed above. The transport via the zeolite pores decreases with temperature both because the activated diffusion is

intrinsically slower at lower temperatures, but also because the high adsorbed loading slows down the diffusion as it is increasingly more difficult to make successful jumps from site-to site at high adsorbed loadings [31, 32].

In summary, the modeling work shows that it is mainly the adsorption properties that dictate the observed trend with increasing selectivity with decreasing temperature and that pressure drop had an adverse effect on membrane performance whereas the effect of concentration polarization was small.

## 5. Conclusions

In the present work, ultra-thin MFI membranes were evaluated for CO<sub>2</sub>/CH<sub>4</sub> separation in the temperature range 250–300 K. The membranes were CO<sub>2</sub>-selective in the entire temperature range and the selectivity towards CO<sub>2</sub> increased with decreasing temperature, which was ascribed to stronger CO<sub>2</sub> adsorption at lower temperatures. The highest CO<sub>2</sub>/CH<sub>4</sub> separation factor of *ca.* 10 was observed at the lowest temperature studied of 247 K. The measured CO<sub>2</sub> permeance, ranging from about 60 to 90 mol s<sup>-1</sup> m<sup>-2</sup> Pa<sup>-1</sup> was the highest ever reported for CO<sub>2</sub>/CH<sub>4</sub> separation using zeolite membranes. Pressure drop over the support had an adverse effect on membrane performance whereas concentration polarization was small at the conditions studied.

## Acknowledgements

The Swedish Research Council Formas (Grant no. 213-2013-1684), the County Administrative Board - Länsstyrelsen i Norrbotten (Grant no. 303-9733-13) and Bio4Energy are gratefully acknowledged for providing financial support for this work.

## References

1. Eze, J.I. and K.E. Agbo, *Maximizing the potentials of biogas through upgrading*. Am. J. Sci. Ind. Res, 2010. **1**(3): p. 604-609.
2. Sandstrom, L., E. Sjöberg, and J. Hedlund, *Very high flux MFI membrane for CO<sub>2</sub> separation*. Journal of Membrane Science, 2011. **380**(1-2): p. 232-240.
3. *BP Statistical Review of World Energy*. 2016; 65th [Available from: <http://www.bp.com/content/dam/bp/pdf/energy-economics/statistical-review-2016/bp-statistical-review-of-world-energy-2016-natural-gas.pdf>].

4. Baker, R.W. and K. Lokhandwala, *Natural gas processing with membranes: An overview*. Industrial & Engineering Chemistry Research, 2008. **47**(7): p. 2109-2121.
5. Makaruk, A., M. Miltner, and M. Harasek, *Membrane biogas upgrading processes for the production of natural gas substitute*. Separation and Purification Technology, 2010. **74**(1): p. 83–92.
6. Bauer, A., et al., *Biogas upgrading-Review of commercial technologies*. 2013, SGC Rapport.
7. Korelskiy, D., et al., *Efficient ceramic zeolite membranes for CO<sub>2</sub>/H<sub>2</sub> separation*. Journal of Materials Chemistry A, 2015. **3**(23): p. 12500-12506.
8. Dortmund, D. and K. Doshi, *Recent Developments in CO<sub>2</sub> Removal Membrane Technology*. UOP LLC: Des Plaines, IL, 1999.
9. Basu, S., et al., *Membrane-based technologies for biogas separations*. Chemical Society Reviews, 2010. **39**(2): p. 750-768.
10. Krishna, R., et al., *Diffusion of CH<sub>4</sub> and CO<sub>2</sub> in MFI, CHA and DDR zeolites*. Chemical Physics Letters, 2006. **429**(1-3): p. 219-224.
11. Kosinov, N., et al., *High flux high-silica SSZ-13 membrane for CO<sub>2</sub> separation*. Journal of Materials Chemistry A, 2014. **2**(32): p. 13083-13092.
12. Tian, Y.Y., et al., *Synthesis of a SAPO-34 membrane on macroporous supports for high permeance separation of a CO<sub>2</sub>/CH<sub>4</sub> mixture*. Journal of Materials Chemistry, 2009. **19**(41): p. 7698-7703.
13. van den Bergh, J., et al., *Natural gas purification with a DDR zeolite membrane; permeation modelling with maxwell-stefan equations*. From Zeolites to Porous Mof Materials: The 40th Anniversary of International Zeolite Conference, Proceedings of the 15th International Zeolite Conference, 2007. **170**: p. 1021-1027.
14. S., Y., et al., *DDR-type zeolite membrane synthesis, modification and gas permeation studies*. Journal of Membrane Science, 2016. **505**: p. 194-204.
15. Poshusta, J.C., R.D. Noble, and J.L. Falconer, *Temperature and pressure effects on CO<sub>2</sub> and CH<sub>4</sub> permeation through MFI zeolite membranes*. Journal of membrane science, 1999. **160**(1): p. 115-125.
16. Sandström, L., J. Lindmark, and J. Hedlund, *Separation of methanol and ethanol from synthesis gas using MFI membranes*. Journal of Membrane Science, 2010. **360**(1): p. 265-275.
17. Hedlund, J., et al., *High-flux MFI membranes*. Microporous and Mesoporous Materials, 2002. **52**(3): p. 179-189.
18. Korelskiy, D., et al., *Characterization of flow-through micropores in MFI membranes by permoporometry*. Journal of Membrane Science, 2012. **417**: p. 183-192.

19. Yu, L., et al., *Very high flux MFI membranes for alcohol recovery via pervaporation at high temperature and pressure*. Separation and Purification Technology, 2015. **153**: p. 138-145.
20. Korelskiy, D., et al., *High flux MFI membranes for pervaporation*. Journal of Membrane Science, 2013. **427**: p. 381-389.
21. Ye, P.C., et al., *Efficient Separation of N-2 and He at Low Temperature Using MFI Membranes*. Aiche Journal, 2016. **62**(8): p. 2833-2842.
22. Perdana, I., et al., *Effect of external mass transport on permeation in a Wicke-Kallenbach cell*. hemical Engineering Research and Design, 2009. **87**(10): p. 1438-1447.
23. Linton, W.H. and T.K. Sherwood, *Mass transfer from solid shapes to water in streamline and turbulent flow*. Chem. Eng. Prog., 1950. **46**: p. 258.
24. F. T. de Bruijn, et al., *Influence of the support layer on the flux limitation in pervaporation*. Journal of Membrane Science, 2003. **223**(1-2): p. 141-156.
25. Jareman, F., et al., *Modelling of single gas permeation in real MFI membranes*. Journal of Membrane Science, 2004. **236**(1): p. 81-89.
26. Thomas, S., et al., *Investigation of mass transfer through inorganic membranes with several layers*. Catalysis Today, 2001. **67**(1-3): p. 205-216.
27. Johnson, R.W., *The handbook of fluid dynamics*. 1998, Boca Raton, Fla: CRC Press.
28. Myers, A.L. and J.M. Prausnitz, *Thermodynamics of Mixed-Gas Adsorption*. Aiche Journal, 1965. **11**(1): p. 121-+.
29. Krishna, R., *The Maxwell-Stefan description of mixture diffusion in nanoporous crystalline materials*. Microporous and Mesoporous Materials, 2014. **185**: p. 30-50.
30. Ohlin, L., et al., *Adsorption of CO<sub>2</sub>, CH<sub>4</sub>, and H<sub>2</sub>O in Zeolite ZSM-5 Studied Using In Situ ATR-FTIR Spectroscopy*. Journal of Physical Chemistry C, 2013. **117**(33): p. 16972-16982.
31. van de Graaf, J.M., F. Kapteijn, and J.A. Moulijn, *Modeling permeation of binary mixtures through zeolite membranes*. Aiche Journal, 1999. **45**(3): p. 497-511.
32. Krishna, R. and J.M. van Baten, *Maxwell-Stefan modeling of slowing-down effects in mixed gas permeation across porous membranes*. Journal of Membrane Science, 2011. **383**(1-2): p. 289-300.
33. Himeno, S., et al., *Characterization and selectivity for methane and carbon dioxide adsorption on the all-silica DD3R zeolite*. Microporous and Mesoporous Materials, 2007. **98**(1-3): p. 62-69.
34. Harlick, P.J.E. and F.H. Tezel, *Adsorption of carbon dioxide, methane and nitrogen: pure and binary mixture adsorption for ZSM-5 with*

- SiO<sub>2</sub>/Al<sub>2</sub>O<sub>3</sub> ratio of 280*. Separation and Purification Technology, 2003. **33**(2): p. 199-210.
35. Chmelik, C., J. van Baten, and R. Krishna, *Hindering effects in diffusion of CO<sub>2</sub>/CH<sub>4</sub> mixtures in ZIF-8 crystals*. Journal of Membrane Science, 2012. **397**: p. 87-91.
  36. Grahn, M. and J. Hedlund, *Maxwell-Stefan modeling of high flux tubular silicalite-1 membranes for CO<sub>2</sub> removal from CO<sub>2</sub>/H<sub>2</sub> gas mixtures*. Journal of Membrane Science, 2014. **471**: p. 328-337.
  37. Ohlin, L. and M. Grahn, *Detailed Investigation of the Binary Adsorption of Carbon Dioxide and Methane in Zeolite Na-ZSM-5 Studied Using in Situ ATR-FTIR Spectroscopy*. Journal of Physical Chemistry C, 2014. **118**(12): p. 6207-6213.



# PAPER II

---

**Ultra-thin MFI membranes with different Si/Al ratios for CO<sub>2</sub>/CH<sub>4</sub> separation**

Liang Yu, Shahpar Fouladvand and Jonas Hedlund

*Manuscript*



## Ultra-thin MFI membranes with different Si/Al ratios for CO<sub>2</sub>/CH<sub>4</sub> separation

Liang Yu\*, Shahpar Fouladvand and Jonas Hedlund

Chemical Technology, Luleå University of Technology, SE-971 87 Luleå, Sweden

\*Corresponding author: Email address: liang.yu@ltu.se; Tel.: +46-920-49-3002; fax: +46-920-49-1199;

### Abstract

Ultra-thin MFI zeolite membranes with different Si/Al ratios (>140, 50 and 25) have been prepared on graded  $\alpha$ -alumina supports and evaluated for separation of equimolar CO<sub>2</sub>/CH<sub>4</sub> mixtures at varying temperatures. The thickness of all membranes was less than 500 nm and permoporometry showed that the amount of defects was very low in the two membranes with highest Si/Al ratio (>140 and 50). The membrane with the lowest ratio (25) also had very few defects in the mesopore range, but comprised a few macropore defects. At room temperature, the Si/Al>140 membrane with the thickness of 350 nm showed very high CO<sub>2</sub> permeance of  $142 \times 10^{-7} \text{ mol s}^{-1} \text{ m}^{-2} \text{ Pa}^{-1}$ , but low separation factor of 1.4. The membrane with a Si/Al ratio of 50 had almost the same thickness, but CO<sub>2</sub> permeance was decreased to  $98 \times 10^{-7} \text{ mol s}^{-1} \text{ m}^{-2} \text{ Pa}^{-1}$ , meanwhile a higher separation factor of 2 was observed at room temperature. For the Si/Al=25 membrane, the CO<sub>2</sub> permeance was  $71 \times 10^{-7} \text{ mol s}^{-1} \text{ m}^{-2} \text{ Pa}^{-1}$  and the separation factor was 3.1 at room temperature. These results indicate that lower Si/Al ratio results in higher separation factor at room temperature, probably due to more extensive CO<sub>2</sub> adsorption on the more polar zeolite. Consequently, as the temperature was reduced from room temperature, all membranes displayed higher separation factor, probably due to increased CO<sub>2</sub> adsorption. However, the membranes displayed different trends. For the two membranes with highest Si/Al ratio, maximum separation factor was observed at the lowest investigated temperature, *i.e.* 250 K, while the membrane with lowest Si/Al ratio displayed a maximum in separation factor at 271 K. The maximum observed separation

factors were 2.6 (at 250 K), 7.1 (at 249 K) and 3.3 (at 271 K) for Si/Al ratios of >140, 50 and 25, respectively. These observations are consistent with an adsorption-diffusion separation mechanism. However, concentration polarisation and mass transfer resistance in the support may also influenced the results.

**Keywords:** ultra-thin MFI zeolite membrane, Si/Al ratio, CO<sub>2</sub>/CH<sub>4</sub> separation, high permeance, natural gas, biogas

## 1. Introduction

Natural gas and biogas containing mainly CH<sub>4</sub> and CO<sub>2</sub> are environmentally friendly fuels and feed stocks. However, CO<sub>2</sub> reduces the heating value, cause pipe corrosion and occupies volume in the delivery pipeline etc. Consequently, removal of CO<sub>2</sub> from biogas and natural gas is necessary and timely research topic [1].

Removal of CO<sub>2</sub> from CH<sub>4</sub> can be achieved by e.g., pressure swing adsorption, cryogenic separation, alkanolamine absorption or membrane separation etc. [2]. Absorption or adsorption processes are the main current techniques for CO<sub>2</sub> separation in industry, but these techniques are costly. Consequently, the application of membrane technology for gas separation has recently attracted much attention [1]. Despite much progress in the development of polymer membranes, the industrial use is limited due to the low permeance and limited robustness of these organic materials [3]. Inorganic zeolite membranes with porous framework and high stability have therefore raised much attention. The well-defined porous zeolite framework may potentially give both high permeance, which reduces the required membrane area and also high selectivity [4].

Several types of zeolite membrane have been investigated for CO<sub>2</sub> separation from CH<sub>4</sub>. Small-pore zeolite membranes, like CHA, DDR with high selectivity but very low CO<sub>2</sub> permeance, namely  $0.4\text{--}5 \times 10^{-7} \text{ mol s}^{-1} \text{ m}^{-2} \text{ Pa}^{-1}$ , have been reported [5-9]. Zeolite membranes with larger pore size, for example MFI and FAU, have also been reported for CO<sub>2</sub>/CH<sub>4</sub> separation showing higher

permeance ( $7.5\text{-}9 \times 10^{-7} \text{ mol s}^{-1} \text{ m}^{-2} \text{ Pa}^{-1}$ ) and separation selectivities in the range of 5-40 [10-12]. We have developed a masking technique which enables preparation of ultra-thin MFI zeolite membranes with limited invasion of zeolite into the support on open graded  $\alpha$ -alumina discs [13]. The membranes have high Si/Al of 139 and displaying a high mixture gas  $\text{CO}_2$  permeance of  $45 \times 10^{-7} \text{ mol s}^{-1} \text{ m}^{-2} \text{ Pa}^{-1}$  and good  $\text{CO}_2/\text{CH}_4$  separation of 4.5 at 10 bar feed pressure and 277 K [14].

MFI zeolite can be prepared with different Si/Al ratios. The amount of aluminium found in the Al atoms included MFI zeolite framework play an important role, as they exert strong electrostatic interactions on ions, polar and quadrupolar molecules. Many systematic studies on the influence of Si/Al ratio on the performance of the zeolite have been reported. As an example, the affinity of  $\text{CO}_2$  molecules to different Si/Al ratio MFI frameworks has been studied by Tuanny et al. [15]. The  $\text{CO}_2$  adsorption/desorption isotherms showed that ZSM-5 zeolites with lower Si/Al ratio has higher affinity for  $\text{CO}_2$  molecules, since the substitution of tetravalent Si atoms for trivalent Al ones into the ZSM-5 develops a charge deficit in the zeolite lattice. In order to maintain the net neutrality, the introduction of other cations is necessary. Therefore, there are more charged sites on the surface as the Si/Al ratio of the zeolite decreases. Interactions among these charged sites on the surface of the ZSM-5 zeolites and the large quadrupole moment of  $\text{CO}_2$  have been pointing out as the factor which is responsible for the good adsorption capacity found in the zeolite. Our group has also reported a detailed investigation of the binary adsorption of carbon dioxide and methane in Na-ZSM-5 as a function of gas composition and temperature [16]. The adsorption selectivity is dependent on the composition, and selectivities in the range 15-31 were observed at 308 K. Furthermore, the adsorption selectivity was increasing with decreasing of temperature and for an equimolar mixture at atmospheric pressure, adsorption selectivities of about 8 and 15 were observed at 393 and 308 K, respectively. Systematic investigations on how membrane performance is affected by the Si/Al ratio have also been reported. The enhancement of the Al-content, *i.e.* decreasing Si/Al ratio, in MFI-crystals of a membrane not only changes its hydrophilic/hydrophobic permeation properties, the stability against acids, and the catalytic activity etc. The Al content also has mainly influenced on the permeation properties of MFI film [17]. MFI membranes with Si/Al ratios of 57 and  $\infty$  were prepared by

Noack et al. [18]. The membranes were characterized by *n*/*i*-pentane and H<sub>2</sub>/SF<sub>6</sub> mixture permeation measurements under various conditions. The ZSM-5 membrane with the highest Al content (Si/Al = 57) separated H<sub>2</sub>/SF<sub>6</sub> mixtures with the separation factor of 51 but not for *n*/*i*-pentane mixtures. Meanwhile, it was also observed that with an enhanced Al content in MFI membranes, the transport resistance is increased by the presence of charge-balancing cations. The results also showed that the increasing of Al content simultaneously increasing concentrations of intercrystalline defect pores is formed. Therefore, the intercrystalline permeance increased with increasing Al content and therefore the mixture selectivities were low for Al-rich MFI membranes [17]. By use of intergrowth supporting substances (ISS) the MFI crystal surface is re-charged and the crystal intergrowth was improved, thereby resulting in higher quality of membranes [19]. We have reported the influence of Si/Al ratio on separation of hydrocarbon isomers [20]. Membranes with the same thickness and similar and low amount of defects were selected for the study. The membranes were prepared from synthesis mixtures with aluminium free, and with a Si/Al ratio of 100, respectively. When the temperature was varied, the membranes showed similar separation trends for butanes, but clear differences were observed for hexanes separation. The differences were assigned to differences in adsorption properties of the membranes.

We have also investigated the permeation of small molecules through MFI films on porous graded  $\alpha$ -alumina discs with a thickness of about 550 nm [21]. Probably due to narrower effective pore diameter for the ZSM-5 membranes (Si/Al = 62) with sodium ions in the zeolite pores, the average hydrogen permeance was 27% lower and the average H<sub>2</sub>/SF<sub>6</sub> single gas permeance ratio was 67% higher comparing with ZSM-5 membranes with higher Si/Al ratio of 157. We have also reported that these membranes showed different performance for separation of methanol and ethanol from synthesis gas [22]. The highest measured methanol/hydrogen separation factor, 32, was observed for more polar membrane with the lowest Si/Al ratio, while the highest ethanol/hydrogen separation factor, 46, was observed for less polar membrane with the highest Si/Al ratio, both at room temperature.

In the present work, ultra-thin MFI membrane on porous graded  $\alpha$ -alumina discs with different Si/Al ratios (the Si/Al ratio in the membrane synthesis mixture are

$\infty$ , 50 and 25) have for the first time been evaluated for equimolar CO<sub>2</sub>/CH<sub>4</sub> separation as a function of temperature.

## 2. Experimental

### 2.1 Membrane Preparation

Porous graded  $\alpha$ -alumina discs (Fraunhofer IKTS, Germany) were used as supports. The diameter is 25 mm and the top layer is 30  $\mu$ m thick with a pore size of 100 nm, the base layer is 3 mm thick with a pore size of 3  $\mu$ m. A suspension of 1 wt% 50 nm silicalite-1 crystals was used as seeds. Prior to seeding, the support was masked as described in a pending patent application [23].

For the zeolite membrane with Si/Al > 140, a synthesis mixture free from aluminium and with a molar composition of 3TPAOH: 25SiO<sub>2</sub>: 1450H<sub>2</sub>O: 100EtOH was used. The growth of zeolite film was carried out by reflux at 88 °C for 55 h. For the membrane with Si/Al=50, aluminium isopropoxide ( $\geq 98.0\%$ , Aldrich) was used as aluminium source and sodium hydroxide (NaOH,  $\geq 99.0$ , Merk) was used to increase the basicity of the solution. The final molar composition of the synthesis mixture was 3TPAOH: 0.25Al<sub>2</sub>O<sub>3</sub>: Na<sub>2</sub>O: 25SiO<sub>2</sub>: 1600H<sub>2</sub>O: 100EtOH and the zeolite films were grown in an oil bath at 100 °C for 22 h under reflux. A synthesis solution with a molar composition of 3TPAOH: 0.5Al<sub>2</sub>O<sub>3</sub>: Na<sub>2</sub>O: 25SiO<sub>2</sub>: 1600H<sub>2</sub>O: 100EtOH was used for preparation of a membrane with a Si/Al ratio of 25, by hydrothermal treatment at 150 °C for 14 h in an autoclave. Finally, the membranes were rinsed in a 0.1 M NH<sub>3</sub> solution and then calcined at 500 °C for 6 h at a heating rate of 0.2 °C min<sup>-1</sup> and a cooling rate of 0.3 °C min<sup>-1</sup>.

The membranes were characterized by *n*-hexane/helium adsorption-branch permoporometry to evaluate the amount of the defects [24]. A detailed description of the experimental and data evaluation procedures are given our in previous work [25]. A scanning electron microscope (SEM, FEI Magellan 400 field emission XHR-SEM) was used to investigate the morphology and microstructure of the membranes. XPS (X-Ray Photoelectron Spectroscopy) was employed to investigate the Si/Al ratio of the MFI membrane. The XPS

spectra were collected with a Kratos Axis Ultra DLD electron spectrometer using monochromated Al K $\alpha$  source operated at 120 W. Analyser pass energy of 160 eV for acquiring wide spectra and a pass energy of 20 eV for individual photoelectron lines were used. The surface potential was stabilized by the spectrometer charge neutralization system. The binding energy (BE) scale was referenced to the C 1s line of aliphatic carbon, set at 285.0 eV. Processing of the spectra was accomplished with the Kratos software.

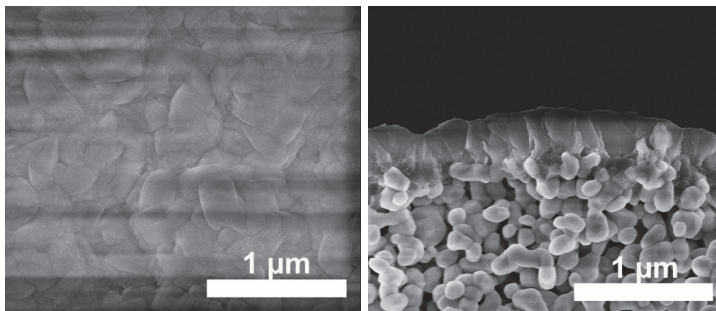
## 2.2 Gas separation experiments

Before separation experiments, the membrane mounted in a steel cell was dried in a flow of helium at 300 °C for 6 h with a heating rate of 1 °C/min followed by natural cooling. Sub-ambient membrane temperatures were achieved by putting the membrane cell in a silicone oil bath. Permeation of gas mixtures was performed in a continuous flow mode using an equimolar mixture of CO<sub>2</sub> and CH<sub>4</sub> introduced to the cell by using mass flow controllers. The retentate pressure was controlled by a back pressure regulator. The pressure on both sides of the membrane was monitored by pressure gauges. The feed mixture was fed to the membrane at a total pressure of 700 kPa at a flow rate of 8 l/min, and the permeate was kept at atmospheric pressure. No sweep gas was used. Gas flow in the permeate stream was measured using a bubble flow meter, and the composition of permeate streams was analysed using a GC (490 Micro GC, Agilent).

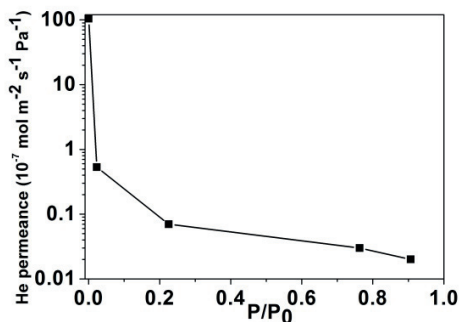
## 3. Results and discussion

Fig. 1 shows cross-section and top view SEM images of an as-synthesised MFI membrane from an aluminium free synthesis solution. The zeolite film is continuous and comprised of well intergrown crystals. Fig. 1 shows that the film is even with a thickness of around 350 nm and that no invasion could be observed by SEM. The single helium gas permeance was  $110 \times 10^{-7} \text{ mol s}^{-1} \text{ m}^{-2} \text{ Pa}^{-1}$ . This high permeance is a result of a thin film on an open, non-invaded graded support. In permoporometry as shown in Fig 2, when *n*-hexane was added to the feed ( $p/p_0 = 0.025$ ), the zeolite pores and microspore defects smaller than about 1.25 nm, were blocked [25] and the helium permeance was dramatically reduced to  $0.53 \times 10^{-7} \text{ mol s}^{-1} \text{ m}^{-2} \text{ Pa}^{-1}$ , *i.e.* it decreased by 99.52 %. When the relative pressure of *n*-hexane was further increased, the helium permeance

through the membrane decreased gradually to  $0.02 \times 10^{-7} \text{ mol s}^{-1} \text{ m}^{-2} \text{ Pa}^{-1}$  at  $p/p_0 = 0.91$ . This indicated that the membrane very high quality, almost no larger pores or defects in line with the SEM observations.



**Fig. 1.** Top view (a) and cross-section (b) SEM images of an as-synthesised MFI membrane from the synthesis solution with  $\text{Si}/\text{Al}=\infty$ .



**Fig. 2.** Permporometry pattern of as-synthesised MFI membrane from the  $\text{Si}/\text{Al}=\infty$  synthesis mixture.

Fig. 3 illustrates the separation results for a feed comprised of an equimolar  $\text{CO}_2/\text{CH}_4$  mixture as a function of temperature for the same membrane. The separation factor and separation selectivity are very similar and increase with the decreasing of temperature. The separation factor was around 1.4 at room temperature and the maximum separation factor was 2.5 at 250 K. The estimated  $\text{Si}/\text{Al}$  ratio for this membrane is 90. The  $\text{CO}_2$  permeance through the membrane was very high of  $142 \times 10^{-7} \text{ mol s}^{-1} \text{ m}^{-2} \text{ Pa}^{-1}$  at room temperature and decreased only slightly to  $106 \times 10^{-7} \text{ mol s}^{-1} \text{ m}^{-2} \text{ Pa}^{-1}$  at the lowest temperature. The low membrane thickness in combination with an open graded support is the main explanation for the high permeance. This permeance is even higher than we

reported previously for MFI membranes with a Si/Al ratio of about 139 [14] and much higher than MFI membranes with similar Si/Al ratio reported by other groups [26-28]. Consequently, the observed CO<sub>2</sub> flux was also very high although the membrane pressure difference was kept relatively low at 6 bar. The flux was 686 kg m<sup>-2</sup> h<sup>-1</sup> at room temperature and 495 kg m<sup>-2</sup> h<sup>-1</sup> at 250 K. The CO<sub>2</sub> and CH<sub>4</sub> permeances and fluxes are generally lower at the lower temperature, probably due to lower diffusivity.

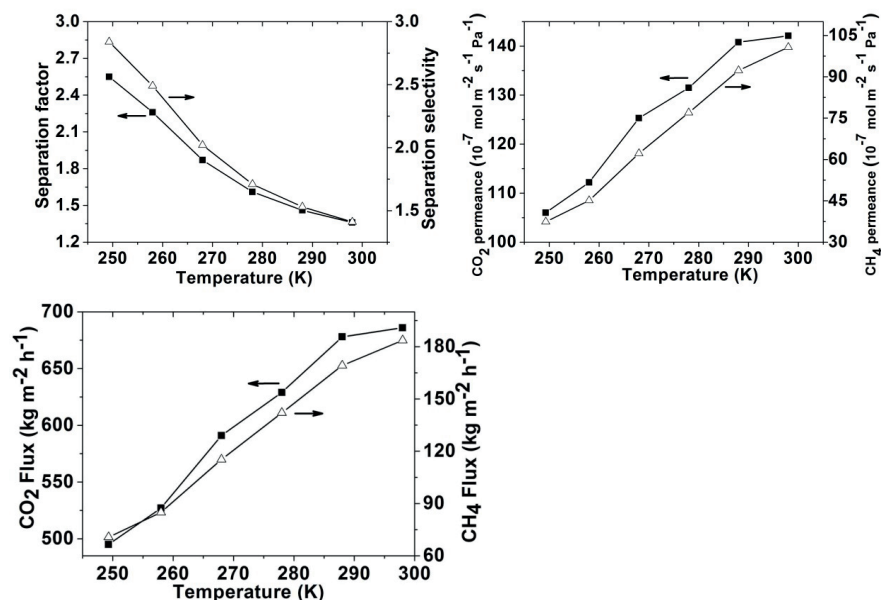


Fig. 3. Separation factor; permeance and flux for separation of an equimolar CO<sub>2</sub>/CH<sub>4</sub> by MFI membrane with Si/Al>140 as a function of temperature.

The membrane prepared by hydrothermal treatment in a synthesis mixture with a Si/Al ratio of 50 has a very similar morphology as the membrane prepared from an aluminium free synthesis mixture as observed from the top-view and cross-section SEM images shown in Fig. 4. The zeolite film is continuous without any crack or pinholes and has almost the same thickness as the membrane prepared from an aluminium free synthesis mixture. Again, the pores of the support were totally open and no invasion could be observed by SEM. The single helium gas permeance was  $98 \times 10^{-7}$  mol s<sup>-1</sup> m<sup>-2</sup> Pa<sup>-1</sup>, i.e. slightly lower than the membrane prepared from an aluminium free synthesis mixture. During permoporometry, the helium permeance decreased by 99.48% when the relative

pressure of n-hexane, *i.e.*  $p/p_0$ , increased from 0 to 0.025 as shown in Fig. 5. This also indicated a high quality of membrane.

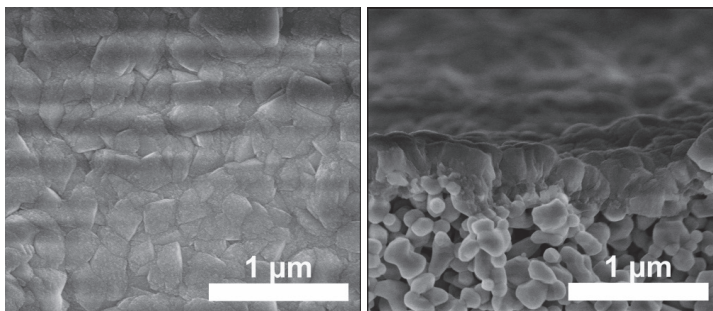


Fig. 4. SEM images of an as-synthesised MFI membrane from the Si/Al=50 synthesis mixture, (a) top view; (b) cross-section.

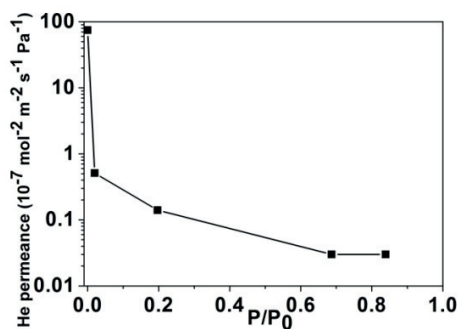


Fig. 5. Permporometry pattern of MFI membrane from the Si/Al=50 synthesis mixture.

Fig. 6 shows the separation results for equimolar  $\text{CO}_2/\text{CH}_4$  gas mixture by Si/Al=50 membrane. At room temperature, the separation factor and separation selectivity were 2, which is higher than for the membrane with a Si/Al ratio exceeding 90. When the temperature was decreased to 250 K, the separation factor was increased to 7, which was around 3 times higher than for the membrane with an Si/Al ratio =90. The  $\text{CO}_2$  permeance was slightly lower than for the membrane with a Si/Al ratio >140 and was  $98 \times 10^{-7} \text{ mol s}^{-1} \text{ m}^{-2} \text{ Pa}^{-1}$  at room temperature. The estimated Si/Al ratios are 46. The higher separation factor compared with the membrane with an Si/Al ratio of >140 membrane is probably a result from the stronger adsorption of  $\text{CO}_2$ . This is due to more aluminium in zeolite framework can produce more polar sites, therefore,  $\text{CO}_2$  molecules need to overcome more energy barrier to go through the higher

aluminium content zeolite pores [29, 30]. For this membrane, the CO<sub>2</sub> flux was 437 kg m<sup>-2</sup> h<sup>-1</sup> at room temperature, and with the decreasing of temperature the permeances and fluxes of CO<sub>2</sub> and CH<sub>4</sub> decreased, probably due to the lower diffusivity.

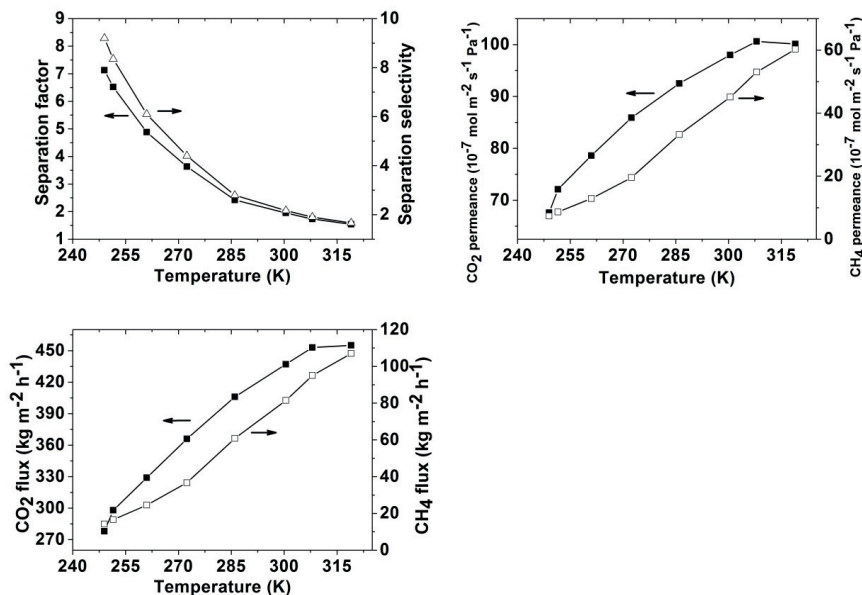


Fig. 6. The separation results for an equimolar CO<sub>2</sub>/CH<sub>4</sub> feed as a function of temperature by Si/Al=50 MFI membrane (a) separation factor; (b) permeance and (c) flux.

Representative SEM images of a membrane prepared from a synthesis mixture with a Si/Al ratio of 25 are shown in Fig. 7. The membrane is continuous and the zeolite film is even with a thickness of around 750 nm, *i.e.* about 2 times thicker than the membranes with high Si/Al ratios as described above. The single helium gas permeance was  $66 \times 10^{-7}$  mol s<sup>-1</sup> m<sup>-2</sup> Pa<sup>-1</sup>, *i.e.* lower than for the thinner films, as expected. The morphology of this membrane appeared different; the zeolite crystals were larger with well-defined grain boundaries. It has been previously reported that pinholes form more frequently in films with well-developed crystals and grain boundaries [31]. However, the permoporometry pattern in Fig. 8 shows that the membrane has reasonably good quality. When n-hexane was added and  $p/p_0$  was increased to 0.025, the helium permeance decreased by 99.07% as compared to 99.52% and 99.48% for the membranes discussed above. Also, the permeance measured at the highest relative pressure of 0.9 was as high as  $0.3 \times 10^{-7}$  mol s<sup>-1</sup> m<sup>-2</sup> Pa<sup>-1</sup>, which indicates that existence of

a few large defects most likely pinholes in the membrane. The large defects could be larger than 48 nm calculated from the Harkins–Jura and Kelvin equation as the description in our previous report [24]. Consequently, the quality of the membrane was not as high as the two membranes with higher Si/Al ratio.

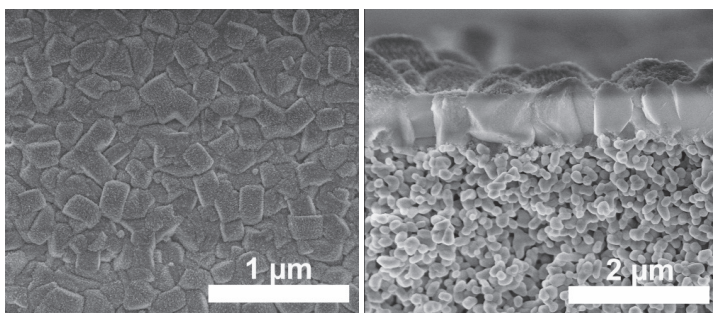


Fig. 7. SEM images of top view (a) and cross-section; (b) of an as-synthesised MFI membrane from the Si/Al=25 synthesis mixture.

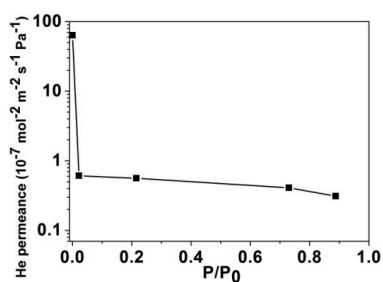


Fig. 8. Permporometry pattern of MFI membrane from the Si/Al=25 synthesis mixture.

The data for separation of an equimolar CO<sub>2</sub>/CH<sub>4</sub> mixture are shown in Fig. 9a. The separation factor was 3.1 at room temperature, which was much higher than the separation factors 1.4 and 2 observed for the membranes with Si/Al ratios of 90 and 46, respectively. In this case, the trend of separation factor as a function of temperature was different as compared to the membranes discussed above. In this case, the separation factor was first increasing when the temperature was decreased down to 271 K, again probably due to increased CO<sub>2</sub> adsorption. Consequently, a maximum in separation factor of 3.3 was observed at 271 K, and lower separation factors were observed as the temperature was reduced further. The estimated Si/Al ratio for this membrane is 21. The higher concentration of aluminium is likely increasing the CO<sub>2</sub> adsorption, resulting in a higher separation factor at room temperature, as compared to the other two

membranes with higher Si/Al ratio. The membrane was probably saturated with CO<sub>2</sub> at 271, where maximum separation factor was observed. A further reduce in temperature, was only resulting in reduced diffusivity of CO<sub>2</sub> and consequently a reduced separation factor. The CO<sub>2</sub> permeance was  $71 \times 10^{-7} \text{ mol s}^{-1} \text{ m}^{-2} \text{ Pa}^{-1}$  at room temperature, which was lower than for the membranes with Si/Al ratios >140 and 50. However, this membrane was about twice as thick as the two membranes with higher Si/Al ratio, which probably is the main cause for the lower permeance. Still, the permeance is much higher than reported MFI zeolite membranes with similar or low Si/Al ratio and much higher than for polymeric membranes [32,33].

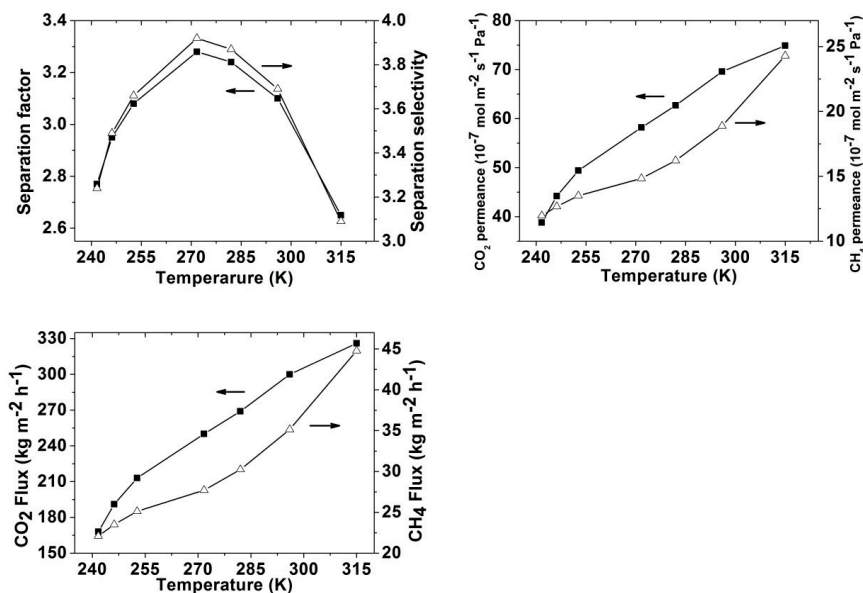


Fig. 9. The separation results of separation factor (a), permeance (b) and flux (c) by Si/Al=25 membrane for an equimolar CO<sub>2</sub>/CH<sub>4</sub> feed as a function of temperature.

Our previous research showed that the performances of our high flux membranes are adversely affected by both concentration polarization and pressure drop over the support. For example in the work by Shahpar et al. high flux MFI membranes were evaluated for separation of equimolar CO<sub>2</sub>/CH<sub>4</sub> using very similar conditions as in this work. At 271 K, the CO<sub>2</sub> permeance and selectivity were about  $78 \times 10^{-7} \text{ mol m}^{-2} \text{ s}^{-1} \text{ Pa}^{-1}$  and 6, respectively. At these conditions, the relative pressure drop over the support was 24 % and the concentration polarization index *i.e.* the ratio between concentration of the main

permeating specie at the membrane surface to the concentration in the feed gas bulk was 0.65. The permeance reported in this work is even higher than previous work where we have estimated the effects of concentration polarization and pressure drop over the support for separation of equimolar CO<sub>2</sub>/CH<sub>4</sub> as described above, we believe that these effects may have affected the results reported herein in a similar or probably even worse fashion.

The membranes with the highest Si/Al ratio have the lowest separation factor and the membranes with the lowest Si/Al ratio have the highest at room temperature. With the decreasing of Si/Al ratio, the CO<sub>2</sub> permeance decrease. The differences in the separation performance of these membranes can be explained by the variety of the zeolite framework properties with the increasing of aluminium content. In present work, the separation factor of Si/Al=46 membrane was much higher comparing with Si/Al=90 membrane for separation of equimolar CO<sub>2</sub>/CH<sub>4</sub> mixture separation at the same separation conditions. This is due to the higher aluminium content increasing the affinity of CO<sub>2</sub> to zeolite framework [17], therefore CO<sub>2</sub> will move even slow with even high aluminium content. Meanwhile, higher aluminium content also indicated that higher Na<sup>+</sup> content in zeolite framework which will probably reduce the accessibility of the pore space [15]. Both effect parameters will be showed up by low permeance in zeolite membrane separation process. In addition, the tendency of the separation factor as a function of the temperature for Si/Al=21 membranes were significantly different with the membranes which have higher Si/Al ratio. This is indicated that the CO<sub>2</sub> adsorption on the feed side was saturated at 271 K for the lowest Si/Al ratio membrane in this study due to even stronger affinity of the zeolite framework to CO<sub>2</sub> molecules. Therefore the adsorption selectivity of the zeolite cannot increase at lower temperature. The CO<sub>2</sub> diffusion rate will be decreased by low temperature, and the lower diffusion of CO<sub>2</sub> leads to the decreasing of the separation factor after 271 K as shown in Fig. 9. For the lower Si/Al ratio membrane, H<sup>+</sup> exchange probably could keep the affinity of the zeolite framework to CO<sub>2</sub> molecules, and meanwhile reduce the effect of Na<sup>+</sup> to make the pore more accessible to have higher permeance [34].

## 5. Conclusions

Ultra-thin MFI zeolite membranes with Si/Al ratios of 90, 46 and 21, were grown on alumina supports. The membranes were evaluated by SEM and permoporometry and for separation of equimolar CO<sub>2</sub>/CH<sub>4</sub> mixtures at different temperatures. With the decreasing of Si/Al ratio, the separation factors were increased and CO<sub>2</sub> permeances were decreased at room temperature. The increased separation factor is probably a result of higher polarity of membranes with low Si/Al ratio of zeolite framework, resulting in increased affinity to CO<sub>2</sub>.

## Acknowledgements

The Swedish Research Council Formas is gratefully acknowledged for financially supporting this work.

## References

- [1] S. Basu, A.L. Khan, A. Cano-Odena, C. Liu, I.F.J. Vankelecom, Membrane-based technologies for biogas separations, *Chem. Soc. Rev.* 39 (2) (2010) 750–768.
- [2] Xiao Yuan Chen, Hoang Vinh-Thang, Antonio Avalos Ramirez, Denis Rodrigue, Serge Kaliaguine, Membrane gas separation technologies for biogas upgrading, *RSC Adv.*, 2015, 5, 24399–24448.
- [3] Richard W. Baker, Kaaeid Lokhandwala, Natural Gas Processing with Membranes: An Overview, *Ind. Eng. Chem. Res.* 2008, 47, 2109–2121.
- [4] Nikolay Kosinov, Jorge Gascon, Freek Kapteijn, Emiel J. M. Hensen, Recent developments in zeolite membranes for gas separation, *Journal of Membrane Science* 499 (2016) 65–79.
- [5] T. Tomita, K. Nakayama, H. Sakai, Gas separation characteristics of DDR type zeolite membrane, *Micropor. Mesopor. Mater.* 68 (1–3) (2004) 71–75.
- [6] Y. Cui, H. Kita, K.I. Okamoto, Preparation and gas separation performance of zeolite T membrane, *J. Mater. Chem.* 14 (5) (2004) 924–932.
- [7] S. Li, M.A. Carreon, Y. Zhang, H.H. Funke, R.D. Noble, J.L. Falconer, Scale-up of SAPO-34 membranes for CO<sub>2</sub>/CH<sub>4</sub> separation, *J. Membr. Sci.* 352 (1–2) (2010) 7–13.

- [8] S. Li, J.G. Martinek, J.L. Falconer, R.D. Noble, T.Q. Gardner, High-pressure CO<sub>2</sub>/CH<sub>4</sub> separation using SAPO-34 membranes, *Ind. Eng. Chem. Res.* 44 (9) (2005) 3220–3228.
- [9] S. Li, J.L. Falconer, R.D. Noble, SAPO-34 membranes for CO<sub>2</sub>/CH<sub>4</sub> separations: effect of Si/Al ratio, *Micropor. Mesopor. Mater.* 110 (2–3) (2008) 310–317.
- [10] Y. Hasegawa, T. Tanaka, K. Watanabe, B.H. Jeong, K. Kusakabe, S. Morooka, Separation of CO<sub>2</sub>–CH<sub>4</sub> and CO<sub>2</sub>–N<sub>2</sub> systems using ion-exchanged FAU-type zeolite membranes with different Si/Al ratios, *Korean J. Chem. Eng.* 19 (2) (2002) 309–313.
- [11] J.C. Poshusta, R.D. Noble, J.L. Falconer, Temperature and pressure effects on CO<sub>2</sub> and CH<sub>4</sub> permeation through MFI zeolite membranes, *J. Membr. Sci.* 160 (1) (1999) 115–125.
- [12] J. Lindmark, J. Hedlund, Modification of MFI membranes with amine groups for enhanced CO<sub>2</sub> selectivity, *J. Mater. Chem.* 20 (11) (2010) 2219–2225.
- [13] J. Hedlund, F. Jareman, A.J. Bons, M. Anthonis, A masking technique for high quality MFI membranes, *J. Membr. Sci.* 222 (2003) 163–179.
- [14] Linda Sandström, Erik Sjöberg, Jonas Hedlund, Very high flux MFI membrane for CO<sub>2</sub> separation, *Journal of Membrane Science* 380 (2011) 232–240.
- [15] Tuanny Santos Frantz, Walter Augusto Ruiz, Cezar Augusto da Rosa, Vanessa Bongalhardo Mortola, Synthesis of ZSM-5 with high sodium content for CO<sub>2</sub> adsorption, *Microporous and Mesoporous Materials* 222 (2016) 209–217.
- [16] Lindsay Ohlin, Philippe Bazin, Frédéric Thibault-Starzyk, Jonas Hedlund, Mattias Grahn, Adsorption of CO<sub>2</sub>, CH<sub>4</sub>, and H<sub>2</sub>O in Zeolite ZSM-5 Studied Using In Situ ATR-FTIR Spectroscopy, *J. Phys. Chem. C* 2013, 117, 16972–16982.
- [17] M. Noack, P. Kölsch, V. Seefeld, P. Toussaint, G. Georgi, J. Caro, Influence of the Si/Al-ratio on the permeation properties of MFI-membranes, *Microporous and Mesoporous Materials* 79 (2005) 329–337.
- [18] M. Noack, G.T.P. Mabande, J. Caro, G. Georgi, W. Schwieger, P. Kölsch, A. Avhale, Influence of Si/Al ratio, pre-treatment and measurement conditions on permeation properties of MFI membranes on metallic and ceramic supports, *Microporous and Mesoporous Materials* 82 (2005) 147–157

- [19] M. Noack, P. Kölsch, A. Dittmar, M. Stöhr, G. Georgi, R. Eckelt, J. Caro, Effect of crystal intergrowth supporting substances (ISS) on the permeation properties of MFI membranes with enhanced Al-content, *Microporous and Mesoporous Materials* 97 (2006) 88–96.
- [20] Fredrik Jareman, Jonas Hedlund, Johan Sterte, Effects of aluminum content on the separation properties of MFI membranes, *Separation and Purification Technology* 32 (2003) 159–163.
- [21] Seyed Alireza Sadat Rezai, Jonas Lindmark, Charlotte Andersson, Fredrik Jareman, Klaus Möller, Jonas Hedlund, Water/hydrogen/hexane multicomponent selectivity of thin MFI membranes with different Si/Al ratios, *Microporous and Mesoporous Materials* 108 (2008) 136–142.
- [22] Linda Sandström, Jonas Lindmark, Jonas Hedlund, Separation of methanol and ethanol from synthesis gas using MFI membranes, *Journal of Membrane Science* 360 (2010) 265–275.
- [23] Soon to be published patent by our group
- [24] J. Hedlund, D. Korelskiy, L. Sandström, J. Lindmark, Permporometry analysis of zeolite membranes, *J. Membr. Sci.* 345 (2009) 276–287.
- [25] D. Korelskiy, M. Grahn, J. Mouzon, J. Hedlund, Characterization of flow-through micropores in MFI membranes by permporometry, *J. Membr. Sci.* 417–418 (2012) 183–192.
- [26] C. Algieri, P. Bernardo, G. Golemme, G. Barbieri, E. Drioli, Permeation properties of a thin silicalite-1 (MFI) membrane, *J. Membr. Sci.* 222 (2003) 181.
- [27] M.C. Lovallo, A. Gouzinis, M. Tsapatsis, Synthesis and characterization of oriented MFI membranes prepared by secondary growth, *AIChE J.* 44 (1998) 1903.
- [28] F. Bonhomme, M.E. Welk, T.M. Nenoff, CO<sub>2</sub> selectivity and lifetimes of high silica ZSM-5 membranes *Micropor. Mesopor. Mater.* 66 (2003) 181.
- [29] Dunne, J. A.; Mariwala, R.; Rao, M.; Sircar, S.; Gorte, R. J.; Myers, A. L. Calorimetric Heats of Adsorption and Adsorption Isotherms. 1. O<sub>2</sub>, N<sub>2</sub>, Ar, CO<sub>2</sub>, CH<sub>4</sub>, C<sub>2</sub>H<sub>6</sub> and SF<sub>6</sub> on Silicalite. *Langmuir* 1996, 12, 5888–5895.
- [30] Dunne, J. A.; Rao, M.; Sircar, S.; Gorte, R. J.; Myers, A. L. Calorimetric Heats of Adsorption and Adsorption Isotherms. 2. O<sub>2</sub>, N<sub>2</sub>, Ar, CO<sub>2</sub>, CH<sub>4</sub>, C<sub>2</sub>H<sub>6</sub>, and SF<sub>6</sub> on NaX, H-ZSM-5, and Na-ZSM-5 Zeolites. *Langmuir* 1996, 12, 5896–5904.

- [31] J.C. Jansen, J.H. Koegler, H. van Bekkum, H.P.A. Calis, CM. van den Bleek, F. Kapteijn, J.A. Moulijn, E.R. Geus, N. van der Puil, Zeolitic coatings and their potential use in catalysis, *Microporous and Mesoporous Materials* 21 (1998) 213-226.
- [32] Haiqing Lin, MiladYavari, Upper bound of polymeric membranes for mixed-gas CO<sub>2</sub>/CH<sub>4</sub> separations, *Journal of Membrane Science* 475(2015)101–109.
- [33] R.W. Baker, B.T. Low, Gas Separation Membrane Materials: A Perspective, *Macromolecules* 47 (2014) 6999–7013.
- [34] Kanna Aoki, Vu A. Tuan, John L. Falconer, Richard D. Noble, Gas permeation properties of ion-exchanged ZSM-5 zeolite membranes, *Microporous and Mesoporous Materials* 39 (2000) 485-492.



# PAPER III

---

## **Efficient ceramic zeolite membranes for CO<sub>2</sub>/H<sub>2</sub> separation**

Danil Korelskiy, Pengcheng Ye, Shahpar Fouladvand, Somayeh Karimi, Erik Sjöberg, Jonas Hedlund

*Journal of Materials Chemistry A*, 3 (2015) 12500-12506





Cite this: *J. Mater. Chem. A*, 2015, **3**, 12500

## Efficient ceramic zeolite membranes for CO<sub>2</sub>/H<sub>2</sub> separation

D. Korelskiy,\* P. Ye, S. Fouladvand, S. Karimi, E. Sjöberg and J. Hedlund

Membranes are considered one of the most promising technologies for CO<sub>2</sub> separation from industrially important gas mixtures like synthesis gas or natural gas. In order for the membrane separation process to be efficient, membranes, in addition to being cost-effective, should be durable and possess high flux and sufficient selectivity. Current CO<sub>2</sub>-selective membranes are low flux polymeric membranes with limited chemical and thermal stability. In the present work, robust and high flux ceramic MFI zeolite membranes were prepared and evaluated for separation of CO<sub>2</sub> from H<sub>2</sub>, a process of great importance to synthesis gas processing, in a broad temperature range of 235–310 K and at an industrially relevant feed pressure of 9 bar. The observed membrane separation performance in terms of both selectivity and flux was superior to that previously reported for the state-of-the-art CO<sub>2</sub>-selective zeolite and polymeric membranes. Our initial cost estimate of the membrane modules showed that the present membranes were economically viable. We also showed that the ceramic zeolite membrane separation system would be much more compact than a system relying on polymeric membranes. Our findings therefore suggest that the developed high flux ceramic zeolite membranes have great potential for selective, cost-effective and sustainable removal of CO<sub>2</sub> from synthesis gas.

Received 24th March 2015  
Accepted 14th May 2015

DOI: 10.1039/c5ta02152a

[www.rsc.org/MaterialsA](http://www.rsc.org/MaterialsA)

## Introduction

Efficient and sustainable CO<sub>2</sub> separation and capture technologies are currently of tremendous interest for several reasons. Firstly, CO<sub>2</sub> is a greenhouse gas, and combustion of fossil fuels is one of the major sources of CO<sub>2</sub> emissions. Secondly, CO<sub>2</sub> is an undesired component in many industrial gas streams, such as natural gas, biogas (methane produced from biomass), and synthesis gas, including bio-syngas produced by biomass gasification.<sup>1</sup> Removal of CO<sub>2</sub> from syngas is a requirement for further processing, such as production of liquid fuels, *e.g.*, methanol,<sup>2</sup> and hydrogen at refineries, petrochemical plants, and Integrated Gasification Combined Cycle (IGCC) power plants.<sup>3</sup> Today, CO<sub>2</sub> is removed primarily by absorption, *e.g.*, amine scrubbing, which is rather an energy-intensive method with high capital costs.<sup>4</sup> In addition, the used absorbents are corrosive and environmentally unfriendly, and the absorption unit is quite large and complex.

Over the past decades, membrane separation technologies have gained an increasing interest for the reasons of high efficiency, sustainability and low energy consumption. Currently, membranes are considered to be one of the most promising CO<sub>2</sub> separation and capture technologies with great market potential.<sup>4,5</sup> For instance, the amount of energy required for a 90% recovery of CO<sub>2</sub> using an efficient membrane has been

estimated to be *ca.* 16% of the power produced by the power plant,<sup>6</sup> whereas the energy required by an amine absorption/desorption process is *ca.* 50% of the power.<sup>7</sup> From the commercial point of view, polymeric membranes have been the most successful membrane type thus far.<sup>4</sup> For instance, the MTR Polaris™ membranes<sup>8</sup> have been the first commercial polymeric membranes able to separate CO<sub>2</sub> from synthesis gas. Today's best polymeric membranes can achieve CO<sub>2</sub>/H<sub>2</sub> selectivities of 10–12 with a CO<sub>2</sub> permeance of *ca.*  $2 \times 10^{-7}$  mol s<sup>−1</sup> m<sup>−2</sup> Pa<sup>−1</sup> at room temperature.<sup>9</sup> Such a low permeance coupled with the fairly poor selectivity necessitates the use of quite large membrane areas for a given separation task. In addition, polymeric membranes suffer from plasticisation induced by CO<sub>2</sub>, which significantly reduces the membrane selectivity and stability over time.<sup>4</sup>

Among ceramic membranes, zeolite membranes are especially attractive and promising.<sup>5</sup> These membranes are microporous aluminosilicate membranes with a well-defined pore system.<sup>10</sup> Due to the porous structure, zeolite membranes can display much higher fluxes than polymeric membranes,<sup>11</sup> *i.e.*, a much smaller membrane area would be needed for a given separation task. Additionally, ceramic zeolite membranes offer an advantage over polymeric membranes in terms of high chemical and thermal stability.<sup>12</sup>

Despite the great interest in synthesis gas upgrading using membranes, the number of studies devoted to evaluation of zeolite membranes for this application is small.<sup>5</sup> Whereas highly CO<sub>2</sub>-selective zeolite membranes have been developed,

Chemical Technology, Luleå University of Technology, SE-97187 Luleå, Sweden.  
E-mail: [daniel.korelskiy@ltu.se](mailto:daniel.korelskiy@ltu.se)

e.g., SAPO-34 membranes<sup>13</sup> with a CO<sub>2</sub>/H<sub>2</sub> separation factor of 110 at 253 K and a feed pressure of 12 bar, there are only a few reports on high flux zeolite membranes. Our research group has extensive experience in preparing ultra-thin (ca. 0.5–1 µm) high flux MFI zeolite membranes,<sup>14</sup> and these membranes have been evaluated for various gas<sup>2,14–19</sup> and liquid<sup>20</sup> separations. In the present work, these membranes were evaluated for separation of CO<sub>2</sub> from H<sub>2</sub> (CO<sub>2</sub>/H<sub>2</sub> mixtures are typically considered as a model system for synthesis gas<sup>21</sup>) in a wide temperature range of 235–310 K and at a feed pressure of 9 bar.

## Experimental

### Membrane synthesis

Supported zeolite membranes comprised of an H-ZSM-5 film with a thickness of ca. 0.5 µm and a Si/Al ratio of 139 (ref. 17) were prepared as described in detail in our earlier work.<sup>14</sup> A porous graded  $\alpha$ -alumina disc (Fraunhofer IKTS, Germany) was used as the support. Prior to the film synthesis, the supports were masked as described elsewhere<sup>22</sup> and then seeded with colloidal MFI crystals of 50 nm in diameter. The film synthesis was carried out for 36 h at 100 °C in a solution with a molar composition of 3TPAOH : 25SiO<sub>2</sub> : 1450H<sub>2</sub>O : 100C<sub>2</sub>H<sub>5</sub>OH. After the synthesis, the membranes were rinsed with a 0.1 M Ammonia solution for 24 h and then calcined for 6 h at 500 °C at a heating rate of 0.2 °C min<sup>-1</sup> and a cooling rate of 0.3 °C min<sup>-1</sup>.

### Membrane characterisation

Scanning electron microscopy (SEM) characterisation of the membranes was carried out using a Magellan 400 (the FEI Company, Eindhoven, the Netherlands) instrument with no coating. Cross-sections of the membranes were obtained by fracture with a pair of cutting pliers.

X-ray diffraction (XRD) characterisation of the membranes was performed using a PANalytical Empyrean diffractometer equipped with a Cu LFF HR X-ray tube and a PIXcel<sup>3D</sup> detector. The data evaluation was performed using HighScore Plus 3.0.4.

The prepared membranes were also characterised by *n*-hexane/helium permoporometry<sup>15</sup> as described in detail in our earlier work<sup>23</sup> and in brief below. The membranes were sealed in a stainless steel cell using graphite gaskets (Eriks, the Netherlands). In order to remove any adsorbed compounds, the membranes were heated to 300 °C at a heating rate of 1 °C min<sup>-1</sup> and kept at this temperature for 6 h in a flow of pure helium. Permoporometry characterisation was carried out at 50 °C and a total pressure difference across the membrane of 1 bar with the permeate stream kept at atmospheric pressure. The relative pressure of *n*-hexane was raised in a step-wise manner from 0 to ca. 0.4. At each relative pressure, the system was allowed to achieve steady-state. For removing *n*-hexane from the permeate stream, a condenser kept at –40 °C followed by a column packed with activated carbon was used. The permeate volumetric flow rate was measured with a soap bubble flow meter. A detailed procedure for estimation of the relative areas of defects from permoporometry data is given in our earlier

work.<sup>23</sup> In brief, the defect width was calculated from *n*-hexane relative pressure using either the Horváth-Kavazoe equation (micropore range defects) or the Kelvin equation (mesopore range defects). For each defect interval, the average defect width was then calculated. Based on the average defect width, the average helium diffusivity in each defect interval was estimated using the gas-translational model. Knowing the diffusivity, the helium molar flux was further calculated from Fick's law. Finally, the defect area was estimated as the ratio between helium molar flow and flux through the defects in that particular interval.

### Separation experiments

Separation experiments were carried out using an equimolar mixture of CO<sub>2</sub> and H<sub>2</sub>. The membrane was in the same cell as used for the permoporometry experiment. The total feed pressure was kept at 9 bar, whereas the total permeate pressure was atmospheric. All experiments were performed without sweep gas. Prior to the experiments, the membrane was flushed with pure helium for 6 h at 300 °C in order to remove any adsorbed species. The permeate volumetric flow rate was measured with a drum-type gasmeter (TG Series, Ritter Apparatebau GmbH) and the permeate composition was analysed on-line with a mass spectrometer (GAM 400, InProcess Instruments).

The flux of component *i*,  $J_i$  (mol s<sup>-1</sup> m<sup>-2</sup>), was estimated from the measured molar flow of the corresponding component through the membrane,  $F_i$  (mol s<sup>-1</sup>) as

$$J_i = F_i/A,$$

where *A* is the membrane area (m<sup>2</sup>).

The permeance of component *i*,  $\Pi_i$  (mol s<sup>-1</sup> m<sup>-2</sup> Pa<sup>-1</sup>), was calculated from the flux of the corresponding component through the membrane as

$$\Pi_i = J_i/\Delta P_i,$$

where  $\Delta P_i$  (Pa) is the partial pressure difference of component *i* across the membrane.

The separation factor  $\beta_{ij}$  was estimated as

$$\beta_{ij} = (y_i/y_j)/(x_i/x_j),$$

where *x* and *y* are the molar fractions in the feed and permeate, respectively.

The membrane selectivity  $\alpha_{ij}$  was estimated as

$$\alpha_{ij} = \Pi_i/\Pi_j.$$

## Results and discussion

### Membrane characterisation

The fabricated membranes were H-ZSM-5 zeolite films with a Si/Al ratio of about 139 (ref. 17) supported on commercial  $\alpha$ -alumina discs (Fraunhofer IKTS, Germany). The synthesis procedure is described in the Experimental. Cross-sectional and

top-view SEM images of an as-synthesised membrane are shown in Fig. 1. The zeolite film appears to be even with a thickness of *ca.* 0.5  $\mu\text{m}$ . The crystals composing the film are well-intergrown with a size of *ca.* 200 nm. No large defects ( $>5$  nm) could be detected by SEM, indicating high quality of the membrane. Fig. 2 shows an XRD pattern of membrane M2. The detected reflections were solely the expected reflections emanating from MFI zeolite and alumina (the support) indicating that no other phase was present in the membrane.

In order to estimate the amount of defects, the membranes were characterised by *n*-hexane/helium permeporometry<sup>15,23</sup> as described in the Experimental. In this technique, helium permeance through the membrane is measured as a function of *n*-hexane relative pressure. Table 1 reports permeporometry data for membrane M1. The helium permeance at a relative pressure of 0, *i.e.*, the permeance through zeolite pores and

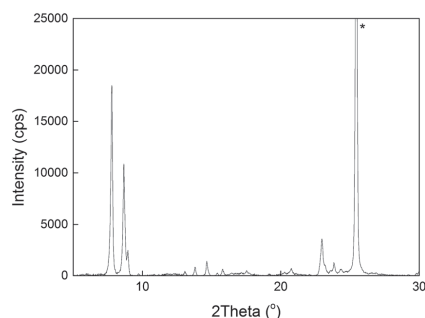


Fig. 2 An XRD pattern of membrane M2. The reflection marked with an asterisk emanates from the alumina support.

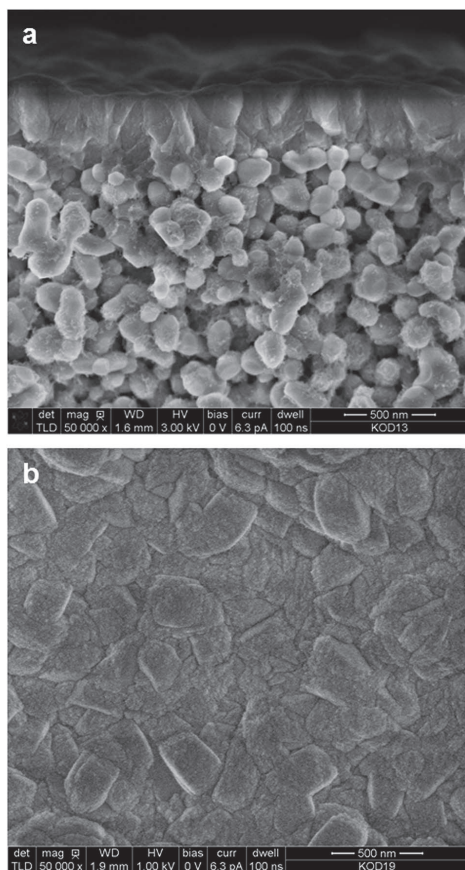


Fig. 1 Cross-sectional (a) and top-view (b) SEM images of an as-synthesised membrane.

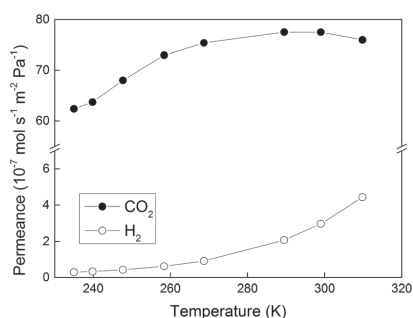
defects, was as high as  $53 \times 10^{-7} \text{ mol s}^{-1} \text{ m}^{-2} \text{ Pa}^{-1}$ , which shows that the zeolite pores are open and rather permeable. As the relative pressure of *n*-hexane was increased, first zeolite pores and then increasingly larger defects were blocked by *n*-hexane, and, therefore, the helium permeance decreased. The amount of defects in terms of relative areas was estimated from the permeporometry data as described in the Experimental. The total amount of defects in the membrane was very low, constituting less than 0.1% of the total membrane area, indicating a very high quality of the membrane. The main type of defects (*ca.* 99.4% of all defects) was micropore defects, *i.e.*, defects  $< 2$  nm in size. Such defects are most likely narrow open grain boundaries, as discussed in detail in our previous work.<sup>24</sup> Essentially no large defects ( $>5$  nm) were detected by permeporometry, which is consistent with the SEM observations.

### Separation experiments

Fig. 3 shows permeances of  $\text{CO}_2$  and  $\text{H}_2$  measured for membrane M1 as a function of temperature when a 50/50 (v/v) mixture of  $\text{CO}_2/\text{H}_2$  was fed to the membrane. The permeance of  $\text{CO}_2$  was high and much greater than that of  $\text{H}_2$  in the entire temperature range. This is a result of the fact that  $\text{CO}_2$  is adsorbing much stronger in the membrane than  $\text{H}_2$ ,<sup>2</sup> thereby blocking the transport of  $\text{H}_2$  and rendering the membrane  $\text{CO}_2$ -selective. The highest  $\text{CO}_2$  permeance of *ca.*  $78 \times 10^{-7} \text{ mol s}^{-1} \text{ m}^{-2} \text{ Pa}^{-1}$  was observed at the higher temperatures, *i.e.*, 290–310 K. In general, the measured  $\text{CO}_2$  permeances were consistent with those previously reported by our group,<sup>2</sup> and one to two orders of magnitude higher than those reported for zeolite and polymeric membranes in the literature. With decreasing temperature, the permeances of both  $\text{CO}_2$  and  $\text{H}_2$  decreased, most likely due to decreasing diffusivity, as discussed in our earlier work.<sup>2</sup> However, the permeance of  $\text{CO}_2$  was reduced to a significantly lower extent than that of  $\text{H}_2$  resulting in increasing selectivity of the membrane to  $\text{CO}_2$  with decreasing temperature, which can be ascribed to increasing adsorption of  $\text{CO}_2$  with decreasing temperature. At the lowest investigated temperature of 235 K, the permeance of  $\text{H}_2$  was as low as  $0.3 \times$

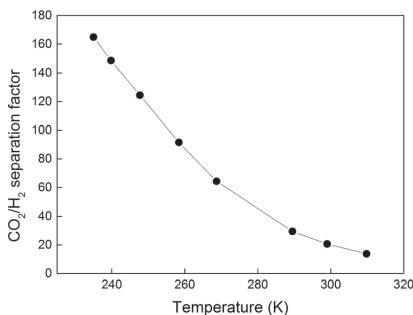
Table 1 Permporometry data for membrane M1

$P/P_0$	He permeance ( $10^{-7}$ mol s $^{-1}$ m $^{-2}$ Pa $^{-1}$ )	Defect interval (nm)	Relative area of defects <sup>a</sup> (%)
0	53	—	—
$3.8 \times 10^{-4}$	1.25	0.71–0.73	0.06
$6.7 \times 10^{-4}$	0.70	0.73–0.80	0.03
$2.1 \times 10^{-3}$	0.36	0.80–1.04	0.01
$1.1 \times 10^{-2}$	0.23	1.04–1.78	0.003
$1.5 \times 10^{-1}$	0.11	1.78–5.43	0
$4.5 \times 10^{-1}$	0.11	>5.43	0.0006
		Total:	0.10

<sup>a</sup> Area of defects per total membrane area.Fig. 3 Permeances of CO<sub>2</sub> and H<sub>2</sub> measured for membrane M1 as a function of temperature.

$10^{-7}$  mol s $^{-1}$  m $^{-2}$  Pa $^{-1}$ , whereas the permeance of CO<sub>2</sub> was still as high as  $62 \times 10^{-7}$  mol s $^{-1}$  m $^{-2}$  Pa $^{-1}$ .

Fig. 4 illustrates CO<sub>2</sub>/H<sub>2</sub> separation factors recorded for membrane M1 as a function of temperature. With decreasing temperature, the separation factor was increasing to as high as 165 at the lowest investigated temperature of 235 K. At these conditions, the CO<sub>2</sub> concentration in the permeate was as high

Fig. 4 CO<sub>2</sub>/H<sub>2</sub> separation factor recorded for membrane M1 as a function of temperature.

as 99.4%. Table 2 shows the CO<sub>2</sub> fluxes, the concentration of CO<sub>2</sub> and H<sub>2</sub> in the permeate stream and the CO<sub>2</sub>/H<sub>2</sub> membrane selectivities. The latter term denotes the ratio of CO<sub>2</sub> and H<sub>2</sub> permeances (not to be confused with the separation factor). The observed CO<sub>2</sub> flux was very high, *i.e.*, 350–420 kg m $^{-2}$  h $^{-1}$ , in the entire temperature range. As discussed in our earlier work,<sup>2</sup> the high CO<sub>2</sub> flux is a result of the very low zeolite film thickness, strong CO<sub>2</sub> adsorption and high CO<sub>2</sub> diffusivity in the zeolite pores, and a relatively high CO<sub>2</sub> partial pressure difference of 3.5 bar across the membrane. The CO<sub>2</sub> flux was decreasing with decreasing temperature, *i.e.*, similar to the CO<sub>2</sub> permeance. Since the membrane was highly CO<sub>2</sub>-selective in the entire temperature range, the CO<sub>2</sub> concentration in the permeate was close to 100%, see Table 2. Consequently, the partial pressure of CO<sub>2</sub> in the permeate was nearly constant at 1 bar, resulting in almost the same partial pressure difference of CO<sub>2</sub> across the membrane (*ca.* 3.5 bar) at all temperatures. As a result, the CO<sub>2</sub> flux was varying with temperature in an almost identical manner as the CO<sub>2</sub> permeance. At 253 K, the separation factor was almost as high as 120 with a CO<sub>2</sub> flux of *ca.* 400 kg h $^{-1}$  m $^{-2}$ , which is 133 times higher than that (3 kg h $^{-1}$  m $^{-2}$ ) reported for the highly CO<sub>2</sub>-selective SAPO-34 zeolite membranes at similar experimental conditions.<sup>13</sup> It is also worth noting that the total duration of the separation experiments was *ca.* 6 h. During this time, the membrane was constantly exposed to a high flow of gas at elevated pressure. Despite this, no indication of deteriorating membrane quality was observed indicating good membrane stability at these experimental conditions. Evaluation of the long-term stability of the membranes would, however, require an industrial gas supply due to the large consumption of gas and the associated high costs, which was beyond the scope of the present work.

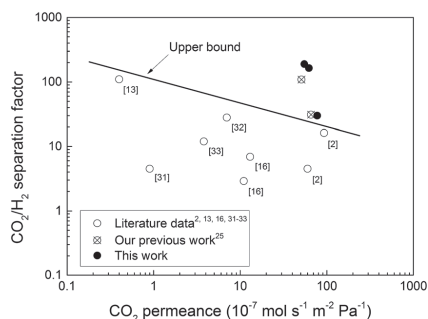
In order to study reproducibility of the separation results, another membrane (denoted M2) with defect distribution similar to that for membrane M1 was evaluated for CO<sub>2</sub>/H<sub>2</sub> separation in the temperature range of 235–270 K using a feed pressure of 9 bar. The separation data for membrane M2 summarised in Table 3 were well comparable to those for membrane M1, illustrating good reproducibility of the separation results.

Table 2 CO<sub>2</sub> flux, permeate concentration and CO<sub>2</sub>/H<sub>2</sub> membrane selectivity observed for membrane M1

$T$ (K)	CO <sub>2</sub> flux (kg h $^{-1}$ m $^{-2}$ )	Permeate concentration (mol%)		CO <sub>2</sub> /H <sub>2</sub> membrane selectivity
		CO <sub>2</sub>	H <sub>2</sub>	
310	423	93.22	6.78	17
300	429	95.36	4.61	26
290	428	96.71	3.28	37
270	420	98.47	1.53	82
260	406	98.91	1.08	117
250	383	99.20	0.80	159
240	364	99.33	0.67	189
235	356	99.40	0.60	210

Table 3 CO<sub>2</sub>/H<sub>2</sub> separation data recorded for membrane M2

<i>T</i> (K)	CO <sub>2</sub> flux (kg h <sup>-1</sup> m <sup>-2</sup> )	CO <sub>2</sub> /H <sub>2</sub> separation factor	CO <sub>2</sub> /H <sub>2</sub> membrane selectivity
270	448	84	107
260	407	114	145
250	404	129	165
240	341	189	242
235	303	202	258

Fig. 5 Summary of the best CO<sub>2</sub>/H<sub>2</sub> separation data reported for zeolite membranes in the literature<sup>2,13,16,31–33</sup> as well as the data obtained in our previous work<sup>25</sup> and in the present work.

A summary of the best CO<sub>2</sub>/H<sub>2</sub> separation data reported for zeolite membranes in the literature is depicted in Fig. 5. Fig. 5 also shows the data obtained in the present work for randomly oriented MFI membranes, and in our previous work<sup>25</sup> for *b*-oriented MFI membranes. The separation performance of the membranes prepared in the present work is well above the upper bound for the best zeolite membranes reported previously. The observed separation performance was also greater than that of high quality *b*-oriented MFI membranes recently prepared by our group.<sup>25</sup> Since the amount of defects in both types of membranes was nearly identical, the difference in the separation performance between the randomly oriented and *b*-oriented MFI membranes should most likely emanate from the

difference in the adsorption affinity of the membranes for CO<sub>2</sub>. The *b*-oriented MFI membranes reported in our previous work<sup>25</sup> were prepared in a fluoride medium at near-neutral pH, whereas the membranes in the present work were synthesised in an alkaline medium. MFI zeolites prepared in a fluoride medium have been shown<sup>26,27</sup> to be less hydrophilic than similar MFI zeolites prepared in a hydroxide medium due to the lower amount of Si–OH groups. In addition, the *b*-oriented MFI-F membranes prepared in our previous work<sup>25</sup> should most probably contain less aluminium in the structure than the present MFI-OH membranes as the leaching of aluminium from the support during the film synthesis should be reduced at near-neutral pH. The lower aluminium content should also result in a less hydrophilic nature of the *b*-oriented MFI-F membranes. At the same time, the adsorption affinity of MFI zeolites for CO<sub>2</sub> has been demonstrated<sup>28–30</sup> to increase with increasing hydrophilicity. Thus, the present randomly oriented MFI-OH membranes, being somewhat more hydrophilic, should have greater adsorption affinity for CO<sub>2</sub> than the *b*-oriented MFI-F membranes, and, hence, should be more selective to CO<sub>2</sub>, as observed in the present work. It is also worth noting that in a previous work<sup>19</sup> we compared randomly oriented MFI membranes prepared in fluoride and alkaline media. A similar trend was observed for CO<sub>2</sub>/H<sub>2</sub> separation, *i.e.*, the MFI-OH membranes were more selective to CO<sub>2</sub> than the MFI-F membranes. In contrast, the latter membranes were more selective to *n*-butanol, as should be expected for a less hydrophilic membrane. It should also be noted that the preparation procedure for the randomly oriented MFI membranes is rather well-established and it is much simpler than that for the *b*-oriented MFI membranes. Hence, at this moment, the randomly oriented high flux MFI membranes should be easier to scale-up.

### Cost estimation

In order to evaluate the economic viability of our membranes, the estimated cost of the membrane modules was compared with that of the commercially available spiral-wound modules used in a natural gas processing plant.<sup>34</sup> The latter modules were assumed to contain MTR Polaris™ membranes recently evaluated for CO<sub>2</sub>/H<sub>2</sub> separation in commercial scale.<sup>3</sup> The zeolite membrane modules were assumed to contain zeolite

Table 4 A comparison between the cost of commercial-scale MTR Polaris™ membrane modules and the cost of modules with high flux MFI membranes prepared in the present work for separation of 300 ton CO<sub>2</sub> per day

Parameter	Polaris membranes	MFI membranes
CO <sub>2</sub> permeance (10 <sup>-8</sup> mol s <sup>-1</sup> m <sup>-2</sup> Pa <sup>-1</sup> )	20 (ref. 3)	775
Module type	Spiral-wound	Multichannel tubes (19 channels)
Membrane area in one module (m <sup>2</sup> )	20 (ref. 3)	10 (ref. 35)
Membrane area needed (m <sup>2</sup> )	395	10
No. of modules needed	20	1
Cost of membranes and module (USD per m <sup>2</sup> )	10 (ref. 34)	2600 <sup>a</sup>
Total cost of modules with membranes (USD)	39 500	26 500

<sup>a</sup> The cost of the module was estimated by Fraunhofer IKTS (Dr Ing. H. Richter, personal communication, 6 March 2015).

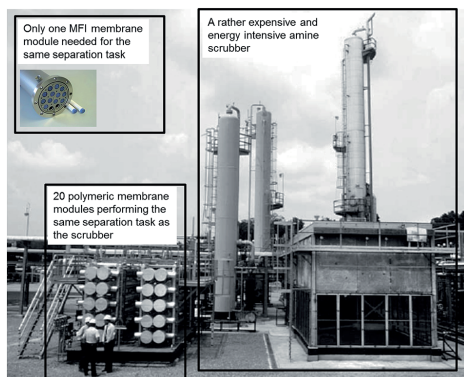


Fig. 6 A comparison between the size of an amine scrubber system, polymeric membrane system and high flux MFI membrane system performing the same separation task. The background picture was adapted from Dortmund and Doshi.<sup>36</sup> The ceramic membrane module image was provided by Inopor®.<sup>35</sup>

membranes supported on 19-channel  $\alpha$ -alumina tubes with the same  $\text{CO}_2$  permeance as measured experimentally for the disc-shaped membranes in the present work. The results of the cost comparison are summarised in Table 4. The costs were estimated for a membrane process with a separation capacity of 300 ton  $\text{CO}_2$  per day at a  $\text{CO}_2$  partial pressure difference across the membrane of 10 bar and room temperature. For this purpose, a polymeric membrane process would need as many as 20 membrane modules, whereas a ceramic MFI zeolite membrane process would only require one module. The estimation demonstrates that the total cost of modules with membranes in the case of high flux MFI membranes was approx. 30% lower than that of high performance commercial polymeric membranes. This is due to the much greater permeance of the MFI membranes resulting in a very low membrane area needed for the separation process. Furthermore, the MFI membranes display much higher  $\text{CO}_2/\text{H}_2$  selectivity (26 and 210 at 300 and 235 K, respectively, see Table 2) than polymeric membranes (10–12 at room temperature). It is also worth noting that the equipment needed for the high flux MFI membrane process will be very compact, as schematically illustrated in Fig. 6. Hence, the prepared MFI membranes have great market potential for separation of  $\text{CO}_2$  from synthesis gas.

## Conclusions

Ultra-thin randomly oriented high flux MFI zeolite membranes were prepared and evaluated for  $\text{CO}_2/\text{H}_2$  separation at a temperature ranging from 235 to 310 K and a feed pressure of 9 bar. The observed membrane separation performance in terms both selectivity and flux was superior to that previously reported for  $\text{CO}_2$ -selective zeolite and polymeric membranes. An initial estimate of the cost of membrane modules revealed that the present membranes were more economically attractive than

commercial-scale polymeric membranes. In addition, the ceramic zeolite membrane separation system would be much more space efficient than a system relying on polymeric membranes. The findings of the present work therefore suggest that the developed high flux MFI zeolite membranes have great potential for selective and cost-effective removal of  $\text{CO}_2$  from synthesis gas.

## Acknowledgements

The Swedish Foundation for Strategic Research (SSF, grant no. RMA08-0018), the Swedish Research Council (VR, grant no. 2010-5317), the Swedish Research Council Formas (Grant no. 213-2013-1684), the Swedish Energy Agency (Grant no. 2013-006587) and Bio4Energy are gratefully acknowledged for financially supporting this work. Amirfarokh Farzaneh is gratefully acknowledged for fruitful discussions.

## Notes and references

- X. Yin, D. Y. C. Leung, J. Chang, J. Wang, Y. Fu and C. Wu, *Energy Fuels*, 2004, **19**, 305–310.
- L. Sandström, E. Sjöberg and J. Hedlund, *J. Membr. Sci.*, 2011, **380**, 232–240.
- H. Lin, Z. He, Z. Sun, J. Vu, A. Ng, M. Mohammed, J. Kniep, T. C. Merkel, T. Wu and R. C. Lambrecht, *J. Membr. Sci.*, 2014, **457**, 149–161.
- S. D. Kenarsari, D. Yang, G. Jiang, S. Zhang, J. Wang, A. G. Russell, Q. Wei and M. Fan, *RSC Adv.*, 2013, **3**, 22739–22773.
- M. Pera-Titus, *Chem. Rev.*, 2013, **114**, 1413–1492.
- T. C. Merkel, H. Lin, X. Wei and R. Baker, *J. Membr. Sci.*, 2010, **359**, 126–139.
- P. Luis, T. Van Gerven and B. Van der Bruggen, *Prog. Energy Combust. Sci.*, 2012, **38**, 419–448.
- Membrane Technology & Research (MTR), <http://www.mtrinc.com>.
- R. W. Baker and B. T. Low, *Macromolecules*, 2014, **47**, 6999–7013.
- J. Caro and M. Noack, *Microporous Mesoporous Mater.*, 2008, **115**, 215–233.
- E. Sjöberg, L. Sandström, O. G. W. Öhrman and J. Hedlund, *J. Membr. Sci.*, 2013, **443**, 131–137.
- J. Caro, M. Noack and E. Stefan, in *Advances in Nanoporous Materials*, Elsevier, 2010, vol. 1, pp. 1–96.
- M. Hong, S. Li, J. L. Falconer and R. D. Noble, *J. Membr. Sci.*, 2008, **307**, 277–283.
- J. Hedlund, J. Sterte, M. Anthonis, A. J. Bons, B. Carstensen, N. Corcoran, D. Cox, H. Deckman, W. de Gijst, P. P. de Moor, F. Lai, J. McHenry, W. Mortier and J. Reinoso, *Microporous Mesoporous Mater.*, 2002, **52**, 179–189.
- J. Hedlund, D. Korelskiy, L. Sandström and J. Lindmark, *J. Membr. Sci.*, 2009, **345**, 276–287.
- J. Lindmark and J. Hedlund, *J. Membr. Sci.*, 2010, **360**, 284–291.
- L. Sandström, J. Lindmark and J. Hedlund, *J. Membr. Sci.*, 2010, **360**, 265–275.

- 18 P. Ye, E. Sjöberg and J. Hedlund, *Microporous Mesoporous Mater.*, 2014, **192**, 14–17.
- 19 H. Zhou, D. Korelskiy, E. Sjöberg and J. Hedlund, *Microporous Mesoporous Mater.*, 2014, **192**, 76–81.
- 20 D. Korelskiy, T. Leppäjärvi, H. Zhou, M. Grahn, J. Tanskanen and J. Hedlund, *J. Membr. Sci.*, 2013, **427**, 381–389.
- 21 M. Grahn and J. Hedlund, *J. Membr. Sci.*, 2014, **471**, 328–337.
- 22 J. Hedlund, F. Jareman, A. J. Bons and M. Anthonis, *J. Membr. Sci.*, 2003, **222**, 163–179.
- 23 D. Korelskiy, M. Grahn, J. Mouzon and J. Hedlund, *J. Membr. Sci.*, 2012, **417–418**, 183–192.
- 24 D. Korelskiy, P. Ye, H. Zhou, J. Mouzon and J. Hedlund, *Microporous Mesoporous Mater.*, 2014, **186**, 194–200.
- 25 M. Zhou, D. Korelskiy, P. Ye, M. Grahn and J. Hedlund, *Angew. Chem., Int. Ed.*, 2014, **53**, 3492–3495.
- 26 Z. Qin, L. Lakiss, L. Tosheva, J.-P. Gilson, A. Vicente, C. Fernandez and V. Valtchev, *Adv. Funct. Mater.*, 2014, **24**, 257–264.
- 27 K. Zhang, R. P. Lively, J. D. Noel, M. E. Dose, B. A. McCool, R. R. Chance and W. J. Koros, *Langmuir*, 2012, **28**, 8664–8673.
- 28 J. A. Dunne, R. Mariwala, M. Rao, S. Sircar, R. J. Gorte and A. L. Myers, *Langmuir*, 1996, **12**, 5888–5895.
- 29 J. A. Dunne, M. Rao, S. Sircar, R. J. Gorte and A. L. Myers, *Langmuir*, 1996, **12**, 5896–5904.
- 30 R. Krishna and J. M. van Baten, *J. Membr. Sci.*, 2010, **360**, 323–333.
- 31 M. Kanazashi, *AIChE J.*, 2008, **54**, 1478–1486.
- 32 K. Kusakabe, T. Kuroda, K. Uchino, Y. Hasegawa and S. Morooka, *AIChE J.*, 1999, **45**, 1220–1226.
- 33 W. J. W. Bakker, F. Kapteijn, J. Poppe and J. A. Moulijn, *J. Membr. Sci.*, 1996, **117**, 57–78.
- 34 R. W. Baker and K. Lokhandwala, *Ind. Eng. Chem. Res.*, 2008, **47**, 2109–2121.
- 35 Inopor®, <http://www.inopor.com>.
- 36 D. Dortmund and K. Doshi, *Chem. Eng. World*, 2003, **38**, 55–66.





